Journal of Molecular Structure 1246 (2021) 131194

Contents lists available at ScienceDirect

Journal of Molecular Structure

journal homepage: www.elsevier.com/locate/molstr

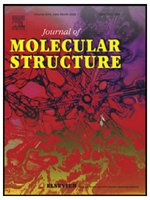

Ru^{3+}, Mn^{2+}, Co^{2+}, Ni^{2+}, Cu^{2+}, and Zn^{2+} uni-metallic complexes of 3-(-(1,5-dimethyl-3-oxo-2-phenyl-2,3-dihydro-1H-pyrazol-4-yl) methylene) hydrazono)indolin-2-one, preparation, structure elucidation and antibacterial activity

Mohamad M.E. Shakdofa[a,*], Quad M. Selim[a], Adel M.E. Shakdofa[b]

[a] *Department of Chemistry, college of Science and Arts at Khulais, University of Jeddah, Jeddah, Saudi Arabia*
[b] *Department of Chemistry, Faculty of Science, Menoufia University, Shebin El-Kom, Egypt*

ARTICLE INFO

Article history:
Received 1 April 2021
Revised 23 June 2021
Accepted 26 July 2021
Available online 31 July 2021

Keywords:
Antibacterial
Dihydrazone
Indolin-2-one
Isatin
Uni-metallic complexes

ABSTRACT

Ru^{3+}, Mn^{2+}, Co^{2+}, Ni^{2+}, Cu^{2+}, Zn^{2+} uni-metallic complexes of dihydrazone derived from the condensation of 3-hydrazonoindolin-2-one with 4-formyl antipyrine were synthesized. The resulted dihydrazone and its chelated compounds structurally characterized basing on spectroscopic tools (NMR, FT-IR, EAS, ESI-MS) thermo-gravimetric, elemental, magnetic and molar conductance measurements. This structural elucidation leads us to conclude that the dihydrazone has been performed as a neutral bidentate chelator linked the Ru^{3+}, Mn^{2+}, Co^{2+}, Ni^{2+}, Cu^{2+}, Zn^{2+} ions via the carbonyl and azomethine of isatin moiety adopting regular or distorted octahedral structures around the central metallic ions. The structural description of dihydrazone and its chelated compounds have been endorsed basing on the Density Functional Theory calculations. The optimized geometry, global reactivity descriptors, and LUMO-HOMO orbitals and of the molecules have been calculated by the DFT-B3LYP method and 6e311G(d,p) basis set. The molecular electrostatic potential picture has been painted utilizing the same level of theory to envision the molecules charge distribution and chemical reactivity. The DFT studies of the designated compounds revealed small HOMO-LUMO gap which is a strong indication to the large reactivity these compounds. The TG analysis has confirmed the complexes chemical formulae and assured that the thermo-degradation processes occur in three or four steps ended with the formation of metal oxide or carbon-contaminated metal oxide residues. The In-vitro antibacterial of dihydrazone and its chelated compounds have been evaluated against *E. coli, P. aeruginosa, K. pneumonia* and *B. subtilis,* the observed antibacterial result denoted that Cu^{2+} and Zn^{2+} complexes have a good activity in comparation with the free dihydrazone.

1. Introduction

Nitrogen-based heterocyclic compounds are important and unique class of organic compounds, they possess physiological and pharmacological properties [1,2] and are constituents of many biologically important molecules, including many vitamins, nucleic acids, pharmaceuticals, antibiotics, dyes, and agrochemicals, amongst many others. In general, these compounds have a role in treatment of Alzheimer's disease, and possess anticancer, antitumor, Free Radical Scavenging activity [3-8]. 1H-indol-2,3-dione (Isatin) is an industrially flexible Nitrogen-based heterocyclic substrate which could be utilized for preparing of a wide variety of heterocyclic, hydrazone and Schiff base compounds as well as a raw material for drug synthesis. They have varied activities comprising antibacterial, antiviral, antimicrobial, antioxidant, antitubercular, anti-HIV, anticancer, and anticonvulsant activities [9-14]. Ammar el al reported that the designated (morpholino-sulfonyl) isatin derivatives showed antitumor properties against CACO, HCT116, MCF-7, and HepG2 cancer cell lines and good inhibition activity against EGFR tyrosine kinase [15]. While the complex of isatin-Schiff base causes cell death in p53-positive tumors [16] while isatin-chromone derivatives have in vitro α-glucosidase inhibitory effect [17]. In addition, the isatin derivatives acted also as a non-toxic corrosion inhibitor for mild steel [18]. Hydrazone chelators were played a crucial part in the development of coordination chemistry while their chelated compounds have been structurally investigated extensively due to their appealing physical and chemical properties, in

---

[*] Corresponding author at: Department of Chemistry, college of Science and Arts at Khulais, University of Jeddah, Jeddah, Saudi Arabia.
E-mail address: mshakdofa@uj.edu.sa (M.M.E. Shakdofa).

https://doi.org/10.1016/j.molstruc.2021.131194

addition to their broad variety of usages in numerous scientific areas comprising anticancer, [19] antitumor [20,21], antibacterial [19], antioxidant [22,23] antimicrobial [24,25], antifungal [26], antiviral [27] anti-tyrosinase [28], and α-glucosidase inhibitors [29] agents. Verma et al reviewed that the hydrazones chelators have anticonvulsant, analgesic, anti-inflammatory, cardio protective, antiplatelet, Antihypertensive and antiprotozoal activities [30,31]. Mono- and bi-nuclear MO_2^{2+} complexes of ONO appended aroyl-hydrazone have in vitro cytotoxicity against lymphoma ascites cell line [32]. Santos el al reported that the acyl-hydrazone of ionized derivatives acted as radical scavenging, myeloperoxidase/acetylcholinesterase inhibitor [33]. The Cu^{2+}complexes of 3,5-dihydroxy-N′-(pyridin-2-ylmethylene)benzohydrazide, 4-methoxy-N′-(pyridin-2-ylmethylene) benzohydrazide, and 2-hydroxy-N′-(1-(pyridin-2-yl) ethylidene)benzo-hydrazide had a significant urease inhibitory activities [34]. Fekri el al reported that the Cu^{2+}, Ni^{2+} and Co^{2+} complexes of N′-(pyridin-2-ylmethylene)benzohydrazide, 2-(2-hydroxybenzylidene)hydrazine-1-carboxamide and 2-(pyridin-2-ylmethylene)hydrazine-1-carboxamide had higher antibacterial and anticancer activities than the parent chelators [35]. Ni^{2+}complexes of benzoyl-hydrazone derivatives are acted as a catalysis for the preparation of 2-aryl-benzoxazoles [36]. Homobinuclear VO^{2+} and Ni^{2+} dihydrazone complexes are acted as a catalysis for the Suzuki-Miyaura cross-coupling and (ep.)oxidation of unsaturated cycloalkene (1,2-cyclohexene) [37]. As a result of the exciting bioactivity of hydrazonic chelators and their complexes and in continuance of our earlier researches, on the designing of bio-effective metal complexes [38-45]. Our objective was to prepare the uni-metallic Ru^{3+}, Mn^{2+}, Co^{2+}, Ni^{2+}, Cu^{2+}, and Zn^{2+} complexes of dihydrazone chelator, 3-(-(1,5-dimethyl-3-oxo-2-phenyl-2,3-dihydro-1H-pyrazol-4-yl) methylene)hydrazono)indolin-2-one (HL). The structure of synthetic compounds was studied via analytical, spectral tools as nuclear magnetic resonance (NMR), infrared (IR), mass spectrum (MS), electronic absorption spectrum (EAS), Density Functional Theory calculations, elemental and thermogravimetric measurements as well as the measurements of molar conductance and magnetic moment for complexes were done. Likewise, the biocidal effect of the synthetic compounds has been assessed against a panel of bacterial strains involving *E. coli, P. aeruginosa, K. pneumonia* and *B. subtilis* basing on agar well diffusion methodology.

2. Experimental

2.1. Physical and analytical measurements

The metal salts, absolute ethanol, DMSO (assay = 99.0-99.8%) were acquired from MERCK company and utilized without any extra purification. 3-hydrazonoindolin-2-one were prepared by a published method [24]. The elemental analyses (C,H,N) of dihydrazone and its chelated compounds have been analyzed at Cairo University, Egypt in the Laboratory of Micro-Analytical, while chloride and metal ions contents have been evaluated by The Standard analytic techniques [46,47]. KBr discs technique was used to measure the IR spectra of the dihydrazone and its chelated compounds on Perkin–Elmer 1430 infrared spectrophotometer in the 400-4000 cm^{-1} range. The EAS in the 200-1100 nm regions have been measured utilizing 1-cm quartz cells in DMSO on a SHMADZU 2600 spectrophotometer. The JEUL JMS-AX-500 mass spectrometer has been utilized for recording the mass spectrum. Brucker Avance 600-DRX spectrometers has been utilized for recording the NMR spectra in DMSO-d_6. The Perkin Elmer 7 Series thermal analyzer has been utilized for recording the thermogravimetric analysis (TG) from 25 to 1000 °C with heating rate 10 °C/min. Gouy Matthey Balance has been has been utilized for measuring the magnetic susceptibilities at 25°C and has been computed by the posted equations [48]. Diamagnetic corrections have been gauged from Pascal's constant [49]. Tacussel type CD6NG conductivity bridge has been utilized for recording the molar conductance of 10^{-3} M solutions (DMSO). The resistance measured in ohms and the molar conductance has been computed by the posted equation [50].

2.2. Synthesis of the dihydrazone

The dihydrazone, 3-(-(1,5-dimethyl-3-oxo-2-phenyl-2,3-dihydro-1H-pyrazol-4-yl) methylene)hydrazono)indolin-2-one (HL) was prepared by mixing the solution of 3-hydrazonoindolin-2-one (161 g, 10 mmol, 40 mL MeOH) with a solution of 4-formyl antipyrine (216, 10 mmol, 30 mL MeOH). The mixture has been refluxed on a water bath for 4 hrs. Then reduce the solution volume to about 40 mL and let it to cool at room temperature. The orange powder which precipitated has been separated out, washed with MeOH, and dried in the void to afford the corresponding **dihydrazone** (**1**) (Fig. 1) (329 mg, 0.916 mmol, 94%) as an orange solid, m.p. 220°C. Elemental analysis (EA) for $C_{20}H_{17}N_5O_2$ (359.39 g /mol): calcd.(Found) %C 66.84 (66.65), %H 4.77 (4.79), %N 19.49 (19.13). IR (KBr, cm^{-1}), 3290, 3173 ν(NH), 3067, 2951, 2831 ν(C-H), 1761 $\nu(^{7}C{=}O^{13})$, 1645 $\nu(^{21}C{=}O^{23})$, 1620 $\nu(^{8}C{=}N^{16})$, 1600 $\nu(^{18}C{=}N^{17})$, 995 $\nu(^{16}N\text{-}N^{17})$. ^{1}H-NMR (600 MHz, DMSO-d_6): δ(ppm) = 10.70 (s, 1H, H^{15}), 8.62 (s, 1H, H^{19}), 8.44 (d, H, H^{9}), 7.42 (m, 1H, H^{10}); 8.16 (m, 1H, H^{11}), 7.60 (d, 1H, H^{12}), 3.39 (s, 3H, $^{28}CH_3$), 2.71 (s, 3H, $^{24}CH_3$), 6.88 (d, 1H, $H^{36\&38}$), 7.35 (dd, 1H, $H^{40\&41}$), 7.02 (m, 1H, H^{42}). ^{13}C-NMR (150 MHz, DMSO-d_6): 153.12(C1), 113.67 (C2), 132.73 (C3), 130.60 (C4), 136.00 (C5), 120.75 (C6), 168.65(C7), 147.47(C8), 162.98(C18), 103.13 (C20), 166.06 (C21), 156.66 (C22), 15.14 (C24), 37.35 (C28), 137.04 (C32), 125.54 (C33), 125.54 (C34), 131.91 (C35), 131.91 (C37), 124.66(C39).

2.3. Preparation of uni-metallic complexes (2-8)

The Ru^{3+}, Zn^{2+}, Cu^{2+}, Ni^{2+}, Co^{2+}, and Mn^{2+} complexes **(2-8)** have been synthesized by mixing the following salts $[RuCl_3].3H_2O$, $[Zn(CH_3COO)_2].2H_2O$, $[Cu(CH_3COO)_2].2H_2O$, $[CuCl_2].2H_2O$ $[Ni(CH_3COO)_2].6H_2O$, $[Co(CH_3COO)_2].6H_2O$ and $Mn(CH_3COO)_2].4H_2O$ (1 mmol, in 50 mL of EtOH) to 3-(-(1,5-dimethyl-3-oxo-2-phenyl-2,3-dihydro-1H-pyrazol-4-yl)methylene) hydrazono)indolin-2-one (HL) (359 mg, 1 mmol, in 30 mL of EtOH). The mixtures have been refluxed for 5 hrs. with stirring. The resultant solid-colored complexes separated out, on heating, washed many times with hot EtOH and ultimately dried in vacuum over P_4O_{10}.

2.3.1. Mn^{2+}-complex (2)

Yield (66.3%), m.p. =290 °C; color: brown; μ_{eff} = 6.03 BM; molar conductivity (Λ_m)=15.4 $ohm^{-1}cm^2mol^{-1}$. EA for $[Mn(HL)(OAc)_2(H_2O)_2].H_2O$, $C_{24}H_{29}MnN_5O_9$, (586.46 g/mol): calcd.(Found) %C 49.15(49.06), %H 4.98(5.23), %N 11.94(11.77), %Mn 9.37(9.07). IR (KBr, cm^{-1}), 3422 $\nu(H_2O)$, 3326, 3196 ν(NH), 3076, 2927, 2815 ν(C-H), 1708 $\nu(^{7}C{=}O^{13})$, 150 $\nu(^{21}C{=}O^{23})$, 1616 $\nu(^{8}C{=}N^{16})$, 2587 $\nu(^{18}C{=}N^{17})$, 1564/1354(210) $\nu_s(CH_3COO)$/ $\nu_{as}(CH_3COO)(\Delta)$, 1022 $\nu(^{16}N\text{-}N^{17})$, 581 $\nu(Co{\leftarrow}O)$, 495 $\nu(Co{\leftarrow}N)$.

2.3.2. Co^{2+}-complex (3)

Yield (63.1%), m.p. >300 °C; color: reddish brown; μ_{eff} = 5.01 BM; Λ_m=11.9 $ohm^{-1}cm^2mol^{-1}$. EA for $[Co(HL)(OAc)_2(H_2O)_2].3H_2O$, $C_{24}H_{33}CoN_5O_{11}$, (626.49 g/mol): calcd.(Found) %C 46.01(45.85), %H 5.31(5.39), %N 11.18(10.91), %Co 9.41(9.43). IR (KBr, cm^{-1}), 3425 $\nu(H_2O)$, 3238 ν(NH), 3047, 2929 ν(C-H), 1721 $\nu(^{7}C{=}O^{13})$, 1650 $\nu(^{21}C{=}O^{23})$, 1620 $\nu(^{8}C{=}N^{16})$, 1576 $\nu(^{18}C{=}N^{17})$, 1557/1340(217) $\nu_s(CH_3COO)$/ $\nu_{as}(CH_3COO)(\Delta)$, 1019 $\nu(^{16}N\text{-}N^{17})$, 522 $\nu(Co{\leftarrow}O)$, 495 $\nu(Co{\leftarrow}N)$.

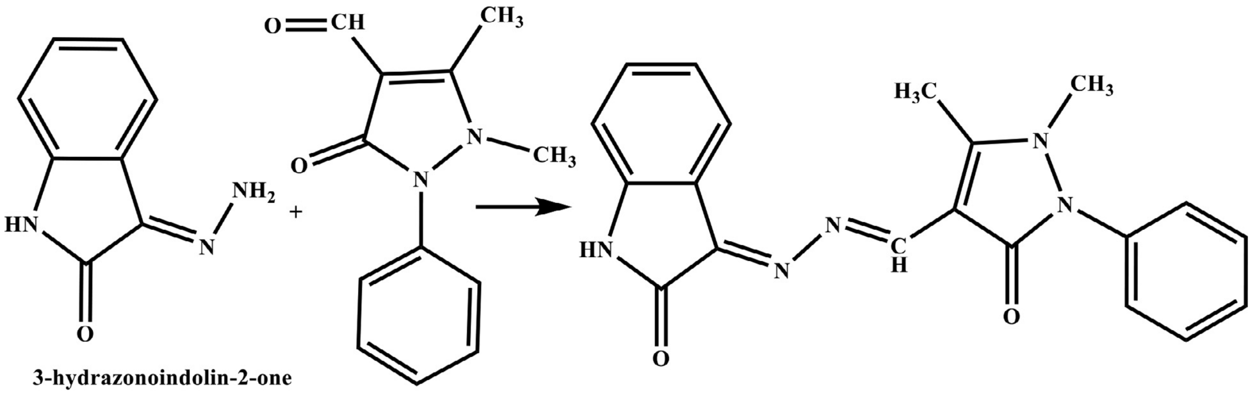

3-hydrazonoindolin-2-one

4-formyl antipyrine

3-(-(1,5-dimethyl-3-oxo-2-phenyl-2,3-dihydro-1H-pyrazol-4-yl)methylene)hydrazono)indolin-2-one

Fig. 1. preparation of the dihydrazone ligand (1)

2.3.3. Ni^{2+}-complex (4)

Yield (69.3%), m.p. =270 °C; color: light Brown; μ_{eff} = 3.03 BM; Λ_m = 13.1 $ohm^{-1}cm^2mol^{-1}$. EA for $[Ni(HL)(OAc)_2(H_2O)_2].H_2O$, $C_{24}H_{29}NiN_5O_9$, (590.22 g/mol): calcd.(Found) %C 48.84(48.52), %H 4.95(5.04), %N 11.87(11.89), %Ni 9.94(10.00). FT-IR (KBr, cm^{-1}), 3411 $\nu(H_2O)$, 3201 ν(NH), 3061, 2932 ν(C-H), 1660 $\nu(^7C{=}O^{13})$, 1645 $\nu(^{21}C{=}O^{23})$, 1619 $\nu(^8C{=}N^{16})$, 1573 $\nu(^{18}C{=}N^{17})$, 1549/1349(200) $\nu_s(CH_3COO)$/ $\nu_{as}(CH_3COO)(\Delta)$, 1027 $\nu(^{16}N\text{-}N^{17})$, 515 $\nu(Ni{\leftarrow}O)$, 452 $\nu(Ni{\leftarrow}N)$.

2.3.4. Cu^{2+}-complex (5)

Yield (60.1%), m.p. >300 °C; color: olive; μ_{eff} = 1.66 BM; Λ_m = 11.3 $ohm^{-1}cm^2mol^{-1}$. EA for $[Cu(HL)(OAc)_2(H_2O)_2]3H_2O$, $C_{24}H_{33}CuN_5O_{11}$, (631.10 g/mol): calcd.(Found) %C 45.68(45.51), %H 5.27(4.99), %N 11.10(11.16), %Cu 10.07(9.77). FT-IR (KBr, cm^{-1}), 3421 $\nu(H_2O)$, 3238 ν(NH), 3063, 2926, 2841, 2778 ν(C-H), 1719 $\nu(^7C{=}O^{13})$, 1643 $\nu(^{21}C{=}O^{23})$, 1618 $\nu(^8C{=}N^{16})$, 1588 $\nu(^{18}C{=}N^{17})$, 1555/1332(229) $\nu_s(CH_3COO)$/ $\nu_{as}(CH_3COO)(\Delta)$, 1032 $\nu(^{16}N\text{-}N^{17})$, 522 $\nu(Cu{\leftarrow}O)$, 475 $\nu(Cu{\leftarrow}N)$.

2.3.5. Cu^{2+}-complex (6)

Yield (56.8%), m.p. >300 °C; color: olive; μ_{eff} = 1.75 BM; Λ_m = 9.1 $ohm^{-1}cm^2mol^{-1}$. EA for $[Cu(HL)_2Cl_2].2H_2O$, $C_{48}H_{39}CuN_{10}O_6$, (889.25 g/mol): calcd.(Found) %C 54.03(54.44), %H 4.31(4.24), %N 15.75(15.32), Cl% 7.79(7.67), %Cu 7.15(6.92). FT-IR (KBr, cm^{-1}), 3416 $\nu(H_2O)$, 3147 ν(NH), 3081, 3001, 2944, 2871 ν(C-H), 1715 $\nu(^7C{=}O^{13})$, 1653 $\nu(^{21}C{=}O^{23})$, 1621 $\nu(^8C{=}N^{16})$, 1520 $\nu(^{18}C{=}N^{17})$, 1012 $\nu(^{16}N\text{-}N^{17})$, 580 $\nu(Cu{\leftarrow}O)$, 480 $\nu(Cu{\leftarrow}N)$.

2.3.6. Zn^{2+}-complex (7)

Yield (53.6%), m.p. =277 °C; color: orange; Λ_m = 8.8 $ohm^{-1}cm^2mol^{-1}$. EA for $[Zn(HL)(OAc)_2(H_2O)_2].2H_2O$, $C_{24}H_{31}ZnN_5O_{10}$, (614.92 g/mol): calcd.(Found) %C 46.88(48.07), %H 5.08(5.14), %N 11.39(11.43), %Zn 10.65(10.78). IR (KBr, cm^{-1}), 3432 $\nu(H_2O)$, 3328 ν(NH), 3077, 2962, 2928, 2814 ν(C-H), 1709 $\nu(^7C{=}O^{13})$, 1655 $\nu(^{21}C{=}O^{23})$, 1613 $\nu(^8C{=}N^{16})$, 1565 $\nu(^{18}C{=}N^{17})$, 1554,1352(202) $\nu_s(CH_3COO)$/ $\nu_{as}(CH_3COO)(\Delta)$, 1012 $\nu(^{16}N\text{-}N^{17})$, 582 $\nu(Zn{\leftarrow}O)$, 503 $\nu(Zn{\leftarrow}N)$. ^1H-NMR (600 MHz, DMSO-d_6): δ(ppm) = 10.88 (s, 1H, H^{15}), 8.42 (s, 1H, H^{19}), 7.52 (d, H, H^9), 7.37 (m, 1H, H^{10}); 8.37 (m, 1H, H^{11}), 7.42 (d, 1H, H^{12}), 3.35 (s, 3H, $^{28}CH_3$), 2.51 (s, 3H, $^{24}CH_3$), 6.92 (d, 1H, $H^{36\&38}$), 7.04 (dd, 1H, $H^{40\&41}$), 6.98 (m, 1H, H^{42}).

2.3.7. Ru^{3+}-complex (8)

Yield (70.7%), m.p. >300 °C; color: brown; μ_{eff} = 1.59; Λ_m =2 7.7 $ohm^{-1}cm^2mol^{-1}$. EA for $[Ru(HL)Cl_3(H_2O)].H_2O$, $C_{20}H_{23}RuN_5O_5Cl_3$, (602.84 g/mol): calcd.(Found) %C 39.85(39.33), %H 3.51(3.82), %N 11.62(11.89), %Cl 17.64(17.23), %Ru 16.77(16.55). IR (KBr, cm^{-1}), 3416 $\nu(H_2O)$, 3139 ν(NH), 3076, 2952, 2840 ν(C-H), 1716 $\nu(^7C{=}O^{13})$, 1663 $\nu(^{21}C{=}O^{23})$, 1618 $\nu(^8C{=}N^{16})$, 1593 $\nu(^{18}C{=}N^{17})$, 1011 $\nu(^{16}N\text{-}N^{17})$, 622 $\nu(Ru{\leftarrow}O)$, 500 $\nu(Ru{\leftarrow}N)$.

2.4. Computational details

The Gaussian 09 Rev. A.02-MSP package program has been used to carry out the Density Functional Theory,[51] and the found data have been imagined by the Gauss View Rev. 5.0.9 software [52]. The dihydrazone molecular structure **(HL)** in the ground state has been optimized utilizing the Density Functional Theory with Beckee3eLeeeYangeParr (B3LYP) functional levels for the 6-311G(d,p) basis set [53,54].

2.5. In vitro antibacterial study

The evaluation of the antibacterial action of the compounds **(1-8)** has been evaluated against *Escherichia coli, (E. coli) Pseudomonas aeruginosa (P. aeruginosa), Klebsiella pneumoniae (K. pneumonia)* and *Bacillus subtilis (B. subtilis)* by agar well diffusion method [55,56]. The bacterial strains have been cultivated on Mueller-Hinton agar at pH 7.4. The plates of agar have been incubated at 37°C for 24 h (bacteria). A negative (DMSO; 2% v/v) and positive controls Tetracycline have been also included to compare the activity. The appearing of inhibition zones has been considered as positive for the existence of antimicrobial action in the test substance. The microbicidal process was carried by agar well diffusion method [55,56]. Therefore, the average of three independent replicates was calculated while the activity index has been calculated by published formula [57].

3. Results and discussion

The chelation of dihydrazone, 3-(-(1,5-dimethyl-3-oxo-2-phenyl-2,3-dihydro-1H-pyrazol-4-yl)methylene)hydrazono)indolin-2-one **(HL) (1)** with the Mn^{2+}, Co^{2+}, Ni^{2+}, Cu^{2+}, and Ru^{3+} salts leading to the formation of steady and colored uni-metallic complexes **(2-8)**. It has found that the designated chelated compounds are non-hygroscopic and insoluble in most organic solvents like acetonitrile, ethanol, methanol, and chloroform and fully soluble in DMF and DMSO. The spectral, analytical, theoretical and analyses data were recorded in Section 2.3,Table 1 & 2. It verified that the chelated compounds **(2-8)** were comprised in molar ratio (1L:1M) which agrees with the expected structures (Figs. 2 & 3).

Table 1
The different quantum chemical parameters of ligand and its complexes (1-8).

No.	E_{HOMO} (eV)	IP	E_{LUMO} (eV)	EA	ΔE (eV)	c (eV)	η(eV)	σ (eV^{-1})	Pi=-c (eV)	W (eV)	ΔN_{max}
HL	-0.2206	0.2206	-0.1060	0.1060	0.1145	0.1633	0.0573	17.46	-0.1633	0.2328	-2.85
(2)	-0.1874	0.1874	-0.1077	0.1077	0.0796	0.1475	0.0398	25.11	-0.1475	0.2733	-3.70
(3)	-0.1740	0.1740	-0.0974	0.0974	0.0766	0.1357	0.0383	26.13	-0.1357	0.2405	-3.54
(4)	-0.2025	0.2025	-0.1094	0.1094	0.0931	0.1560	0.0466	21.48	-0.1560	0.2613	-3.25
(5)	-0.1602	0.1602	-0.1257	0.1257	0.0345	0.1429	0.0173	57.94	-0.1429	0.5917	-8.28
(6)	-0.1805	0.1805	-0.1257	0.1257	0.0548	0.1531	0.0274	36.48	-0.1531	0.4274	-5.58
(7)	-0.1683	0.1683	-0.1286	0.1286	0.0397	0.1484	0.0198	50.40	-0.1484	0.5552	-7.48

Table 2
Some energetic properties of dihydrazone and its complexes calculated by DFT method.

No.	E_{HOMO} (eV)	E_{LUMO} (eV)	Total energy (eV)	binding Energy (a.u.)	Dipole Moment (Debye)
HL	-0.2206	-0.1060	-0.3266	-1197	4.61
(2)	-0.1874	-0.1077	-0.2951	-2957	6.71
(3)	-0.1740	-0.0974	-0.2714	-3189	6.67
(4)	-0.2025	-0.1094	-0.3120	-3314	7.24
(5)	-0.1602	-0.1257	-0.2858	-3447	7.57
(7)	-0.1683	-0.1386	-0.3069	-3585	11.23
(6)	-0.1805	-0.1257	-0.3061	-4954	9.72

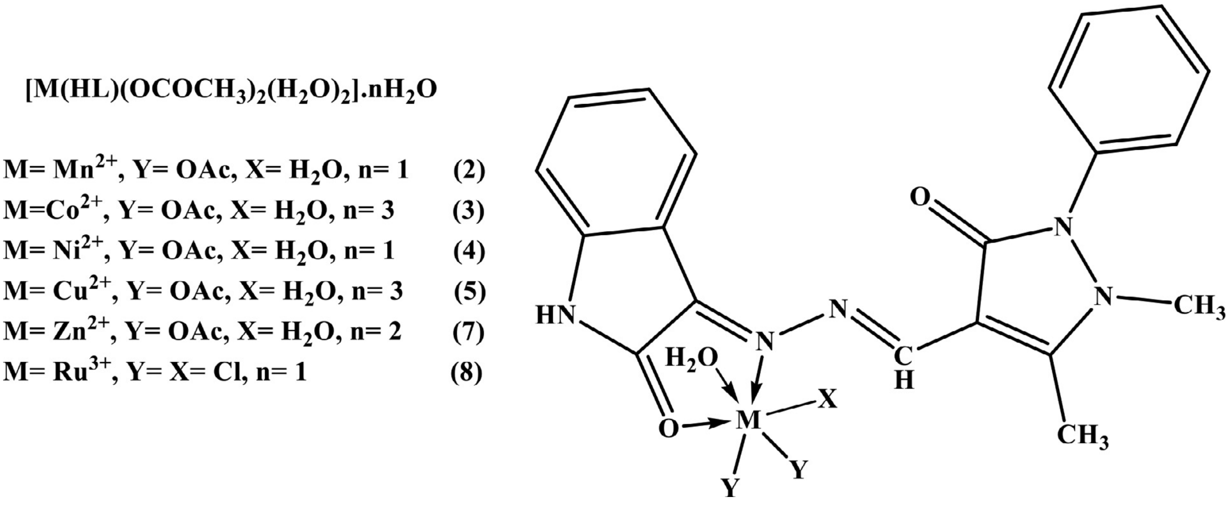

Fig. 2. Structure of uni-metallic Mn2+, Co2+, Ni2+, Cu2+and Ru3+ complexes (2-5) and (7-8).

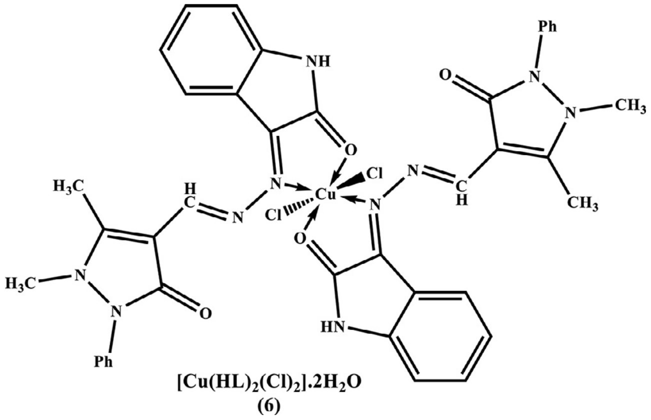

Fig. 3. Structure of uni-metallic Cu2+ complex (6).

3.1. Molar-conductance measurements

The molar conductance of metal chelates **(2-8)** has been carried out in DMSO at concentration 10^{-3} M. All metal chelates **(2-8)** showed molar conductance values between 8.8-33.9 $ohm^{-1}cm^{2}mol^{-1}$, which are within the anticipated range for the non-electrolytic species [58]. This finding signaled to the lack of any anions out of the coordination sphere of all these metals chelates. The significantly high value of complex **(8)** may be due to the preferential solvolysis by DMSO [58].

3.2. Nuclear magnetic resonance

To attain advantageous info about dihydrazone structure and recognition of hydrogen bonding as well as defining its mode of chelation. The experimental ^{1}H and ^{13}C NMR chemical shifts in DMSO–d_6 of the free dihydrazone is outlined in Section 2.2 and explained, basing on the atom labeling in Fig. 4. The ^{1}H-NMR spectrum of dihydrazone **(Supl. 1)** demonstrated two singlets chemical shift at 10.70 and 8.62 ppm which could be attributed to the proton of NH and azomethine groups [59]. These signals were verified by its disappearing in the spectrum with D_2O. In addition, the two singlets chemical shift looked at 3.39 and 2.70 ppm assigning to the to three protons of N–CH_3 and C–CH_3 of antipyrine moiety correspondingly [60]. The protons of indolin-2-one moiety were appeared as doublet at 8.44 ppm and 7.60 ppm assigning to (H-C^6) and (H-C^3) correspondingly [59]. As well as multiples at 7.50 and 7.42 ppm assigning to (H-C^2) and (H-C^1) correspondingly [59]. The

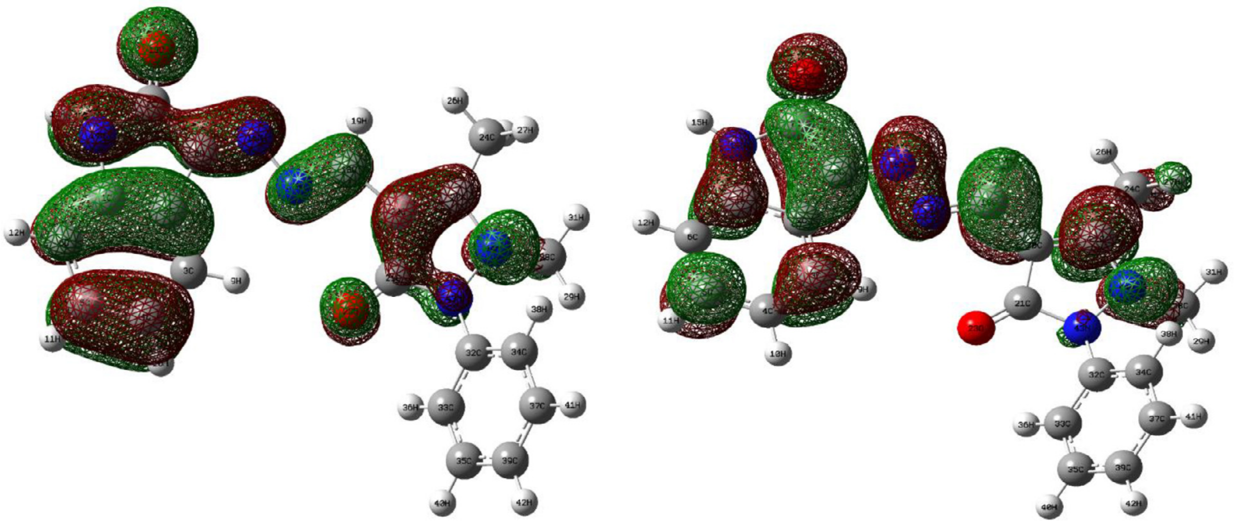

Fig. 4. Fig. 5; The 3D orbital pictures of the HUMO-LUMO level for dihydrazone by the DFT/B3LYP/6e311ppG(d,p).

five protons of phenyl ring of antipyrine moiety were appeared in 6.88-7.35 ppm range [60] . The ^{1}H-NMR spectrum of Zn^{2+} complex showed that the chemical shift of the protons of NH and azomethine ($H^{18}C{=}N^{17}$) groups are appeared at the same position indicating that the NH and azomethine groups did not take part in the chelation to the metallic ions which supported the suggested mode of chelation. The ^{13}C-NMR spectrum of dihydrazone **(Supl. 2)** demonstrated various chemical shift assured the proposed structure of dihydrazone. the number of chemical shifts be like the number of magnetically non-equivalent carbon atoms in the dihydrazone. The two azomethine carbon atoms ($^{13}C{=}N$, $^{9}C{=}N$) were appeared at 162.98 and 147.47 ppm while the two-chemical shift at 168.65 and 166.06 ppm were imputed to carbonyl carbons of the indolin-2-one and antipyrine moieties correspondingly [25,41]. Moreover, the spectrum displayed two signals at 153.12 and 156.66 were imputed to carbon atoms attached the nitrogen of indolin-2-one and pyrazoline moieties (^{4}C-NH, ^{15}C-N) [25,41]. The other carbons of indolin-2-one and phenyl moieties were observed in the 113.67-137.04 ppm range [25,41]. In addition, the spectrum revealed two singlet chemical shift at δ 37.35 and 15.14 ppm imputed to carbon atoms of methyl groups of antipyrine moiety of $N{-}CH_3$ and $C{-}CH_3$ correspondingly [41].

3.3. *Mass spectrum of dihydrazone (MS)*

The MS for dihydrazone **(1)** **(Supl. 3)** verified the anticipated structure with molecular ion peak m/z equal 359. Moreover, The MS demonstrated base peak at m/z = 159 which was allocated to a 2-phenyl-1l2-pyrazol-3(2H)-one. In addition, the MS showed eight fragments which can be explained as follow. The first fragment (a) at m/z 345 due to the losing methyl group from the dihydrazone molecule, the next fragment (b) at m/z =331 owing to the losing of fragment (a) a methyl group, the third fragment (c) at m/z =255 anticipated to the losing of fragment (b) a phenyl moiety. The fourth fragment (d) at m/z =282 which may be due the losing of phenyl moiety from the ligand molecule. Moreover, the other four fragments which appeared at m/z =172, 187, 145 and 216 which may be assigned to the fragments (E)-3-((l3-methylene)hydrazono) indolin-2-one (e), 1,5-dimethyl-2-phenyl-1,2-dihydro-3H-4l3-pyrazol-3-one (f), 3-(l2-azanylidene)indolin-2-one (h) and 4-((l2-azanyl)methyl)-1,5-dimethyl-2-phenyl-1,2-dihydro-3H-pyrazol-3-one (i) correspondingly **(Supl. 3).**

3.4. *FT-IR spectra*

The diagnostic FT-IR data of dihydrazone and its uni-metallic chelated compounds **(1-8)** are depicted in Section 2. The dihydrazone (**HL**) spectrum displayed several weak and broad bands at 3290, 3173, 3067, 2951 and 2831 cm^{-1} which could be ascribed to the stretching vibrations of ν(NH) of the isatin moiety, aromatic and aliphatic C–H correspondingly [61,62]. Likewise the strong bands at 1761 and 1645 could be attributed to the isatin and antipyrine carbonyl groups $\nu(^{8}C{=}O)$[63] $\nu(^{18}C{=}O)$[60] respectively. Whereas the moderate bands at 1620 and 1600 cm^{-1} could be allocated to the azomethine groups [63]. While the bands at 995 cm^{-1} could be owing to ν(N-N)[61]. The bonding mode of the dihydrazone with metallic cations have been elucidated from a comparison between the FT-IR spectra of chelated compounds and that of the free dihydrazone. This comparison displayed that The IR spectral data of all complexes revealed that the bands relating to ν(N-H) of isatin moiety as well as the carbonyl and azomethine of antipyrine moiety appeared around the original position, signaling that these groups did not contribute to the chelation. The FT-IR spectra of all complexes demonstrated that the bands of carbonyl and azomethine groups of isatin moiety are shifted to lower wave numbers and appearing in the ranges 1666-1721 and 1520-1593 cm^{-1} respectively, supportive to the chelation of these groups to metallic ions. The spectra of all complexes revealed also new bands in the 515–622 and 452-503 cm^{-1} ranges which could be assigned to the $\nu(O{\rightarrow}M)$ and $\nu(N{\rightarrow}M)$ respectively [64]. From that data of elemental analyses and FT-IR we can be concluded that the dihydrazone linked the metallic ions as a neutral bidentate chelator via carbonyl and azomethine groups of isatin moiety. In the acetate complexes **(3)** and **(8),** The $\nu_{as}(COO^-)$ and $\nu_s(COO^-)$ of acetate ions were displayed at 1555,1339; 1563,1334 and 1523, 1326 cm^{-1}. The difference between the two values ($\Delta = \nu_{as}$ -ν_s) was 216, 229 and 197 cm^{-1} which is implying that acetate ions bonded to the metallic cations as a uni-dentate ligand [65,66].

3.5. *The electronic absorption spectrum (EAS) and magnetic moment (μ_{eff}) measurements*

The **EAS** of the dihydrazone (**HL**) and its metal chelates **(1-8)** have been recorded in DMF and their data have been summarized in Table 3. The **EAS** of dihydrazone (**HL**) divulged two bands at 265, 295 nm which are owing to $\pi{\rightarrow}\pi^*$ transitions within the phenyl and isatin moieties which is approximately un-

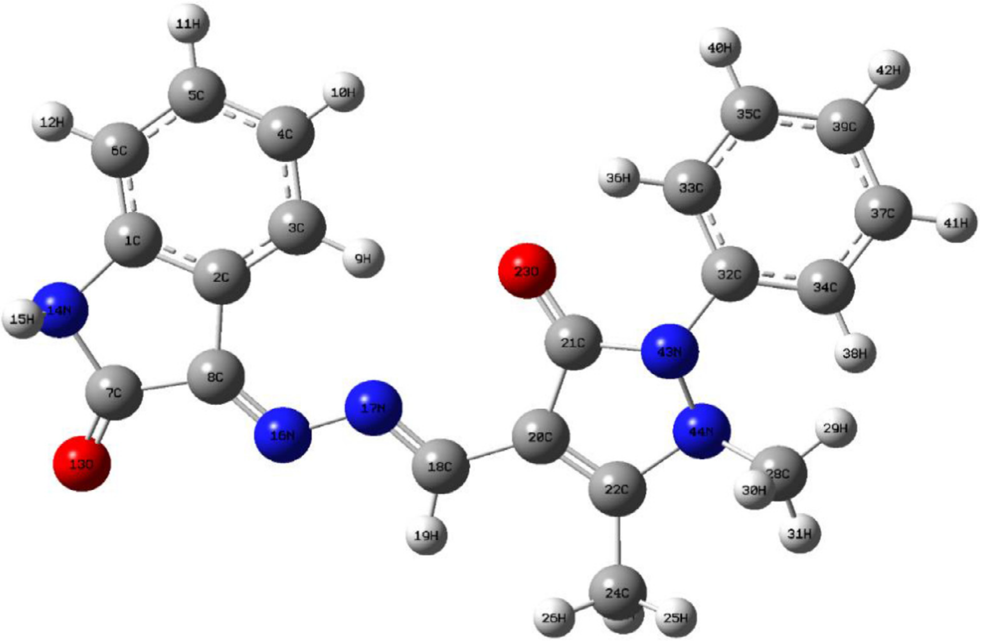

Fig. 5. Fig. 4: The optimized structure of dihydrazone obtained using B3LYP/6-311G(d,p) level for HL.

Table 3
UV-Vis. spectra of the dihydrazone (HL) and its, Ru^{3+}, Mn^{2+}, Co^{2+}, Ni^{2+}, Cu^{2+} and Zn^{2+} complexes (2-8).

No	Bands (nm) in DMSO	Electronic transition	μ_{eff} (BM)	Geometry
HL(1)	265, 280, 318, 380	$\pi\rightarrow\pi^*$, $n\rightarrow\pi$	--	–
Mn^{2+}complex (2)	264, 290, 321, 357, 414, 561, 627, 709, 814	$(\nu_1)^6A_{1g}\rightarrow{}^4T_{1g}(4G)$ $(\nu_2)^6A_{1g}\rightarrow{}^4E_g(4G)$ $(\nu_3)^6A_{1g}\rightarrow{}^4E_g(4D)$ $(\nu_4)\ {}^6A_{1g}\rightarrow{}^4T_{1g}(4p)$	6.03	octahedral
Co^{2+}complex (3)	270, 290, 320, 400, 500, 685, 1088	$(v_1)^4T_1g(F)\rightarrow{}^4T_{2g}(F)$ $(v_2)^4T_1g(F)\rightarrow{}^4A_{2g}$ $(v_3)^4T_1g(F)\rightarrow{}^4T_{1g}(p)$	5.01	distorted octahedral
Ni^{2+}complex (4)	265, 285, 313, 400, 561, 625, 708, 1080	$(\nu_1)^3A_{2g}(F)\rightarrow 3T_2g(F)$, $(v_2)^3A_{2g}(F)\rightarrow{}^3T_{1g}(F)$ $(\nu_3)^3A_{2g}(F)\rightarrow{}^3T_{1g}(P)$	3.03	distorted octahedral
Cu^{2+}complex (5)	269, 298, 325, 400, 688, 1084	$(\upsilon_3)^2B_{1g}\rightarrow{}^2E_g(d_{x2\text{-}y2}\rightarrow d_{xy})$ $(\upsilon_2)^2B_{1g}\rightarrow{}^2A_{1g}\ (d_{x2\text{-}y2}\rightarrow d_{z2})$	1.66	tetragonally distorted octahedral
Cu^{2+}complex (6)	268, 289, 323, 402, 655, 1098	$(\upsilon_1)^2B_{1g}\rightarrow{}^2B_{2g}\ (d_{x2\text{-}y2}\rightarrow d_{yz}\ d_{xz})$	1.75	
Zn^{2+}complex (7)	263, 296, 318, 400	–	Dia.	–
Ru^{3+}complex (8)	265, 282, 313, 405, 606	LMCT ${}^2T_{2g}\rightarrow{}^2A_{2g}$	1.59	octahedral

shifted on chelation. While the two bands which observed at 310, 390 nm probably assigning to $n\rightarrow\pi^*$ transition within the azomethine and carbonyl chromophore imputing that the azomethine nitrogen and carbonyl oxygen participate in the chelation process through the their electron pairs.[59,67,68] The μ_{eff} value of Mn^{2+} complex **(2)** is equal to 6.03 BM. This value anticipated to high spin Mn^{2+} configuration (d^5) [69]. In high-spin octahedral Mn^{2+} complex, the ground state is ${}^6A_{1g}$. Since there are no excited terms for sextet spin multiplicity, d–d transitions are doubly forbidden. But some forbidden transitions happen and therefore, these transitions have an exceptionally low molar extinction coefficient value. So the EAS of Mn^{2+} complexes display four transitions: ${}^6A_{1g}\rightarrow{}^4T_{1g}(4G)(\nu_1)$, ${}^6A_{1g}\rightarrow{}^4E_g(4G)(\nu_2)$, ${}^6A_{1g}\rightarrow{}^4E_g(4D)(\nu_3)$, and ${}^6A_{1g}\rightarrow{}^4T_{1g}(4p)(\nu_4)$ [70,71]. The EAS of Mn^{2+} complex **(2)** displayed four peaks at 814, 709, 627, 561 nm which could be compliant with Mn^{2+}ions in an octahedrally environment (Fig. 2).[70] The ${}^4F$ ground state of Co^{2+} in a sphere of octahedral symmetry is split into ${}^4A_{2g}$, ${}^4T_{2g}$ and ${}^4T_{1g}(P)$ and three spin-allowed transitions $(v_1)^4T_1g(F)\rightarrow{}^4T_{2g}(F)$, $(v_2)^4T_1g(F)\rightarrow{}^4A_{2g}$ and $(v_3)^4T_1g(F)\rightarrow{}^4T_{1g}(p)$ are expected [71,72]. In accordance with this description the presence of three bands in the EAS of Co^{2+} complex **(3)** at 1088, 685 and 500 nm supporting that the Co^{2+} complex **(3)** has an octahedrally structure [Fig. 2]. The low value of ν_1/ν_2 (1.59) ratio regarding the typical range for an octahedral Co^{2+} com-lexes (1.95–2.48), signaling to its distortion. The Co^{2+} complex **(3)** displayed μ_{eff} equal 5.01 BM which is matched with the normal value for high spin octahedral Co^{2+} complexes [73]. The EAS for Ni^{2+} complex displayed three peaks at 1080, 625 and 561 nm can be attributed to the ${}^3A_{2g}(F)\rightarrow 3T_2g(F)(\nu 1)$, ${}^3A_{2g}(F)\rightarrow{}^3T_{1g}(F)(v2)$ and ${}^3A_{2g}(F)\rightarrow{}^3T_{1g}(P)(\nu 3)$ transitions correspondingly which is consistent with an octahedrally structure (Fig. 1) [71,74,75]. The ν_2/ν_1 value is 1.53 which is lower than the typical value for an octahedrally Ni^{2+} complex (1.5–1.75), underlined that, the octahedral geometry of Ni^{2+} complex **(4)** is distorted [74]. The μ_{eff} value for Ni^{2+} complex is 3.03 BM which lies in the range for a d^8 electronic configuration of Ni^{2+} complexes in an octahedral field [76]. In six coordinated (octahedral crystal field) of Cu^{2+} ion, the ground state is $t_{2g}{}^6e_g{}^3$ with ${}^2E_g$ term while the excited state is $t_{2g}{}^5e_g{}^4$ with ${}^2T_{2g}$ term. So, the anticipated electronic transition is ${}^2E_g\rightarrow{}^2T_{2g}$. But because of the Jahn-Teller effect the octahedrally

Table 4
loss The thermogravimetric analysis (TG) of Ru^{3+}, $Mn^{2+}Co^{2+}$, Ni^{2+}, $Cu^{2+}$and Zn^{2+}complexes (2-8).

No.	Temp. range °C	Weight loss (%) Found(calcd.)	assignment	the residue composition
(2)	25-70	2.83 (3.07)	Dehydration process (H_2O)	$[Mn(HL)(CH_3COO)_2(H_2O)_2]$
	70-225	6.60 (6.14)	Loss of two coordinated water molecules	$[Mn(HL)(CH_3COO)_2]$
	225-290	20.75(20.27)	Loss of two acetate ions ($2CH_3COOH$)	[Mn(HL)]
	290-730	56.60(56.37)	Complex decomposition forming MnO+C	MnO+C
(3)	25-105	6.47 (6.83)	Dehydration process ($3H_2O$)	$[Co(HL)(CH_3COO)_2(H_2O)_2]$
	110-180	6.33 (5.75)	Loss of two coordinated water molecules	$[Co(HL)(CH_3COO)_2]$
	200-290	18.72(18.98)	Loss of two acetate ions	[Co(HL)]
	300-660	55.32(54.69)	Complex decomposition forming CoO	CoO
(4)	25-120	3.39 (3.05)	Dehydration process (H_2O)	$[Ni(HL)(CH_3COO)_2(H_2O)_2]$
	120-170	6.78 (6.10)	Loss of two coordinated water molecules	$[Ni(HL)(CH_3COO)_2]$
	170-350	18.64(18.98)	Loss of two acetate ions	[Ni(HL)]
	350-580	53.38(53.98)	Complex decomposition forming NiO+2C	NiO+2C
(5)	25-115	8.66 (8.56)	Dehydration process ($3H_2O$)	$[Cu(HL)(CH_3COO)_2(H_2O)_2]$
	115-165	6.29 (5.71)	Loss of two coordinated water molecules	$[Cu(HL)(CH_3COO)_2]$
	170-282	18.11(18.84)	Loss of two acetate ions	[Cu(HL)]
	282-420	51.97(52.38)	Complex decomposition forming CuO+C	CuO+C
(6)	25-70	4.47(4.05)	Dehydration process ($2H_2O$)	$Cu(HL)_2(Cl)_2]$
	180-320	25.98(25.54)	Loss of two Cl ions and $2C_6H_5$ moieties	$Cu(HL\text{-}Ph)_2]$
	320-600	57.72(58.76)	Complex decomposition forming CuO+2C	CuO+2C
(7)	25-150	5.66(5.86)	Dehydration process ($2H_2O$)	$[Zn(HL)(CH_3COO)_2(H_2O)_2]$
	150-200	6.60(5.86)	Loss of two coordinated water molecules	$[Zn(HL)(CH_3COO)_2]$
	200-400	18.87(19.33)	Loss of two acetate ions	[Zn(HL)]
	400-580	49.06(49.86)	Complex decomposition forming ZnO+3C	ZnO+3C
(8)	25-90	3.10 (2.99)	Dehydration process (H_2O)	$[Ru(HL)(Cl)_3(H_2O]$
	90-200	3.78 (2.99)	Loss of one coordinated water molecule	$[Ru(HL)(Cl)_3]$
	230-280	17.82(17.64)	Loss of three chloride ions	[Ru(HL)]
	280-500	54.26(53.65)	Complex decomposition forming $1/2Ru_2O_3$+C	$1/2Ru_2O_3$+C

structure is deformed either by compression or elongation the octahedron leading to tetragonal symmetry in which the ^2E_g is split into $^2B_{1g}(d_{x2-y2})$ and $^2A_{1g}(d_{z2})$ levels while the $^2T_{2g}$ also splits into $^2B_{2g}(d_{xy})$ and $^2E_g(d_{xz},d_{yz})$ levels. Thus, three bands are expected for tetragonal (D_{4h}) symmetry viz. $^2B_{1g}\leftarrow{}^2A_{1g}$, $^2B_{1g}\leftarrow{}^2B_{2g}$, $^2B_{1g}\leftarrow{}^2E_g$ which can be manifested around 1000, 650 and 500 nm consecutively [71,72,77]. In accordance with the above description the presence of two bands in EAS of Cu^{2+} chelated compounds **(5-6)** at 688, 1084 and 655, 1098 nm ascribed to the transitions $(\nu_1)^2B_{1g}\rightarrow{}^2A_{1g}(d_{x2-y2}\rightarrow d_{z2})$ and $(\nu_2)^2B_{1g}\rightarrow{}^2B_{2g}$ $(d_{x2-y2}\rightarrow d_{xy})$ transitions pointed out that these chelated compounds have a tetragonally distorted octahedral structure (Fig. 2) [71,78-80]. The third band which assigned to the $(\upsilon_3)^2B_{1g}\rightarrow{}^2E_g(d_{x2-y2}\rightarrow d_{xy})$ does not appear here may be due to the boarding of the bands. The Cu^{2+} complexes **(5-6)** displayed μ_{eff} values at 1.66 and 1.75 BM respectively which is associated to spin-only value for Cu^{2+} complexes.[81] The magnetic moment value of Ru^{3+}complex **(8)** is 1.59 BM which is well compatible with d^5 low spin Ru^{3+}complex [81]. The low spin paramagnetic Ru^{3+} complexes, a d^5 system with $^2T_{2g}$ as the ground term originating from the $^5t_{2g}$ configuration and the first excited doublet levels in the order of increasing energy are $^2A_{2g}$ and $^2T_{1g}$, which arise from $^4t_{2g\rightarrow}{}^1e_g$ configuration. Hence, two bands corresponding to $^2T_{2g}\rightarrow{}^2A_{2g}$ and $^2T_{2g}\rightarrow{}^2T_{1g}$ are possible. However, the EAS of Ru^{3+} complex **(8)** displayed one bands at 606 which may be assigned to $^2T_{2g}\rightarrow{}^2A_{2g}$ transition. While the band noticed at 405 nm is possibly because of the charge transfer transitions (LMCT) happening from the filled chelator (HOMO) orbital to the singly occupied ruthenium t_2 orbital (LUMO). The band location is like to those noted for other octahedrally Ru^{3+} complexes [71,82].

3.6. Density Functional Theory (DFT) study

3.6.1. Molecular parameters

As specified by the theorem of Koopman, quantum chemical parameters of the dihydrazone (**HL,1**) and its chelated compounds **(2-8)** have been estimated and their data have been listed in Table 1 [83]. The energy of the lowest un-occupied molecular orbital (E_{LUMO}) acts as an electron recipient and specifying the molecular ability to nucleophilic attacking because it can accept electrons. The outermost highest occupied molecular orbital energy (E_{HOMO}) can act as an electron donor and specifying the molecular ability to electrophilic attacking because it has electrons. The HOMO and LUMO of dihydrazone **(HL)** and its chelated compounds were shown by DFT/B3LYP/6-311G(d,p) calculation and have been displayed in Fig. 4 **and Supls. 4-5**. The negatively and positively zone were specified by green and red colors, consecutively. The HOMO and LUMO regions are spread over the pyrazoline and indole moieties as well as the hydrazonic linkages. The LUMO and HOMO orbitals energies as well as their adjacent orbitals are negative, signifying that the dihydrazone **(HL)** is stable [84]. The dihydrazone chelates metallic ions via the carbonyl oxygen O(13) belongs indole moiety as well as the azomethine nitrogen atom N(16) Fig. 4. These atoms are the active locations for chelation because they are from the highly electronegatively charges atoms. Moreover, these atoms are from the atoms in which the HOMO level is centered on them suggesting that these sites are the favored positions for nucleophilic attack at the metallic cations (Fig. 4). This imply that these locations with high coefficients HOMO density have been directed to the metallic cations [85]. The values of separation energy (**$\Delta E = E_{LUMO}-E_{HOMO}$**) of the compounds **(1-8)** displayed that the chelated compounds **(2-8)** are fewer stable and more active than the dihydrazone **(HL)** [86]. The Ionization potential (**$IP = - E_{HOMO}$**) is the energy essential to eliminate an electron from a molecule [87], while the electron affinity (**$EA = - E_{LUMO}$**) is the energy liberalized when the system earn an extra electron [87]. The absolute hardness (**$\eta = (IP-EA)/2$**) and absolute softness (**$\sigma = 1/\eta$**) can be serve as a measure the resistance of atom to a charge transfer and the ability of an atom or group of atoms to accept electrons respectively [88]. From the values of absolute hardness and absolute softness, it can predict the molecules stability and reactivity. The soft molecules owned a small energy gap

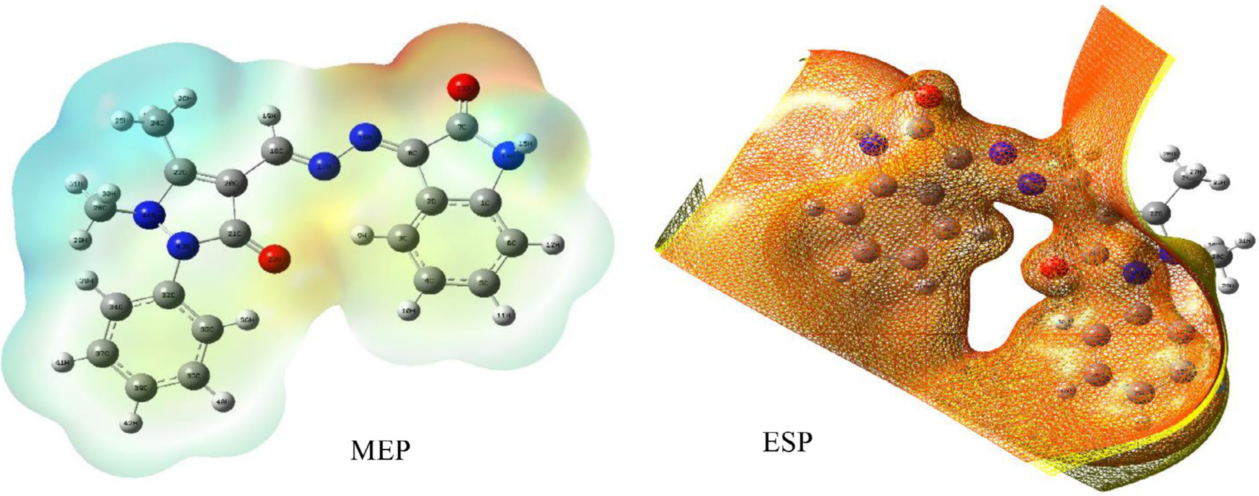

Fig. 6. Molecular electrostatic potential (MEP) and electrostatic potential (ESP) of the dihydrazone (1).

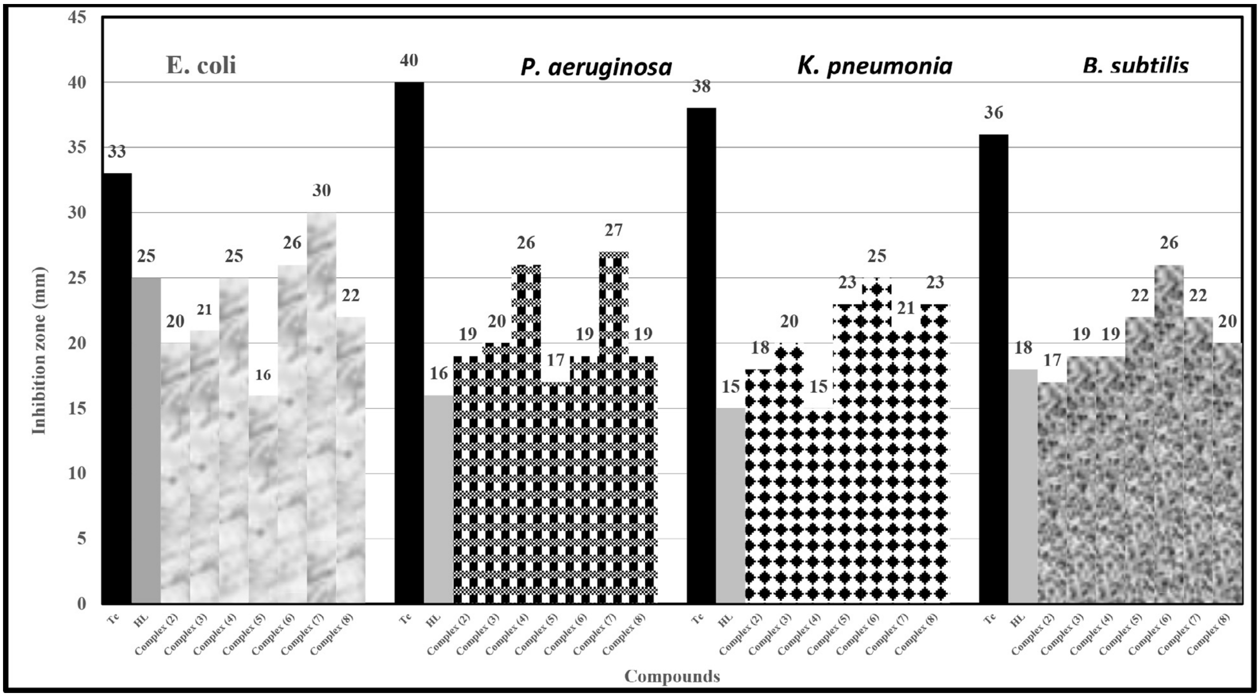

Fig. 7. The Order of antimicrobial activity of the ligand and its complexes.

whereas the hard ones owned a great energy gap. So, the hard molecules are less reactive than the soft ones because of the soft molecules can easily give electrons to a receiver. In the coordination compounds, the metallic cations and ligands can perform as Lewis's acid and Lewis's base respectively, the chelators are the most effective for coordination. Thus, it can be concluded that the chelator with a proper $\boldsymbol{\sigma}$ value has a well tendency to chelate the metallic cations efficiently. This supposition was emphasized by the value of chemical potential ($\mathbf{Pi}= -\chi$) for the chelator [84,85]. From the calculated values of the chemical potentials ($\mathbf{Pi}= -\chi$), absolute electronegativities ($\chi = \mathbf{(IP{+}EA)/2}$), index of electrophilicity ($\boldsymbol{\omega}= \mathbf{Pi}\ ^{2}/(2\eta)$) and reactivity index ($\Delta \mathbf{N_{max}}= -\mathbf{Pi}/\eta$) [89] we can conclude that: i)ΔN_{max} is the stabilization scale for the system energy when the system earns a further electronic charge from the environment, the electrophilicity index (χ) is positive. Certain amount and the direction of the charge transfer is completely determined by the electronic chemical potential (Pi) of the molecule because an electrophile is a chemical species that can accept electrons from the environment and its energy must decrease upon accepting electronic charge. Therefore, its electronic chemical potential must be negative exactly as supported by the values in Table 1. the electrophilicity index (ω) values are small signifying to a good nucleophile. ii) The dihydrazone chelates with the metal ions *via* the carbonyl oxygen atoms O(13) and azomethine nitrogen atoms N(16). These atoms are from the atoms of high electronegative charge, which approves that they are the active locations for chelation iii) The estimated dipole moment value of the ligand **(HL)** is 4.61 Debye is less than that of the complexes **(2-8)** (6.67-11.23 Debye). This may be due the chelation of metallic cations with the dihydrazone (HL) occurred by the carbonyl oxygen and azomethine nitrogen atoms. Other energetic properties of dihydrazone and its complexes were calculated by DFT method and listed in Table 2. The data of table 2 indicated that the complexes binding energy are higher than binding energy the dihydrazone (HL) suggesting

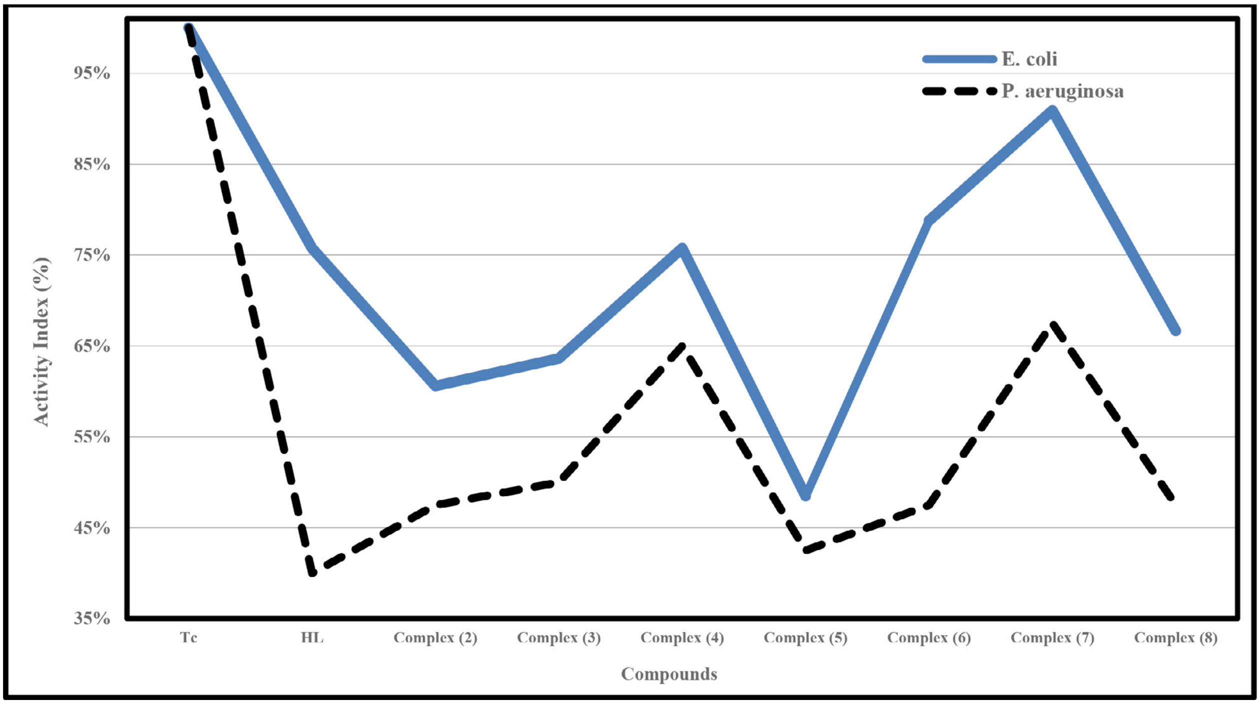

Fig. 8. The activity index of antibacterial activity of the dihydrazone and its complexes against gram-negative bacteria activity.

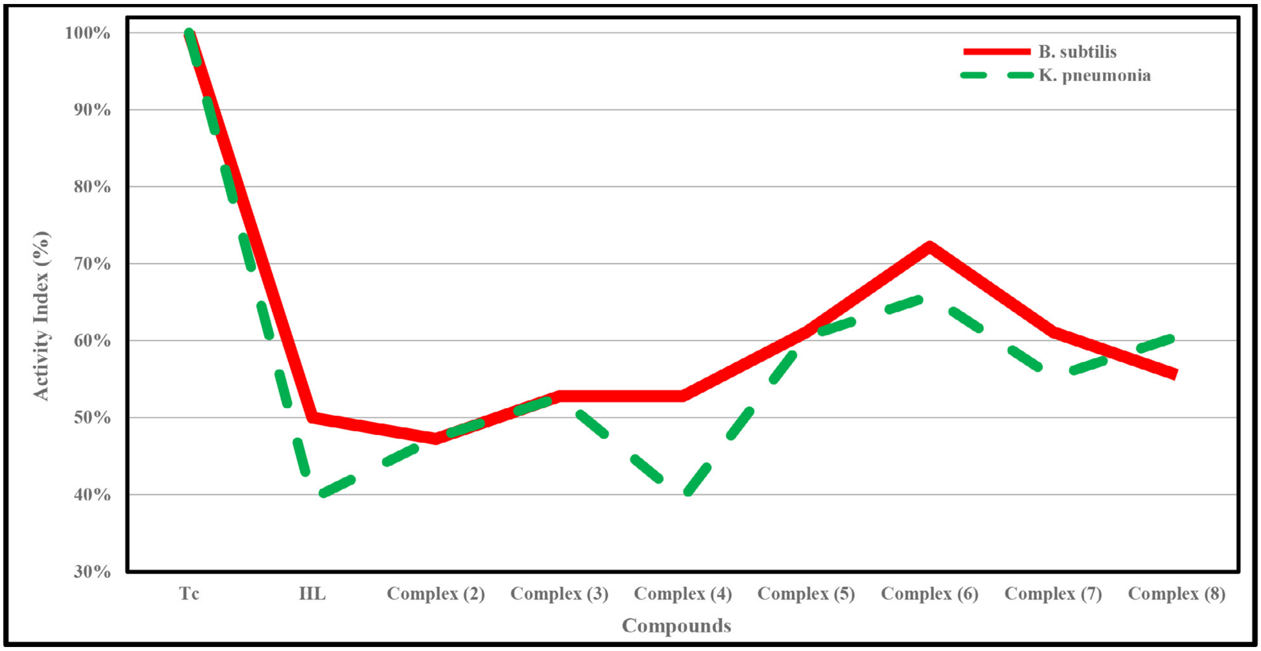

Fig. 9. The activity index of antibacterial activity of the dihydrazone and its complexes against gram-positive bacteria activity.

that the prepared metal complexes are more stable than the dihydrazone (HL) [90].

3.6.2. *Mulliken atomic charges for the dihydrazone (HL,1)*

The Mulliken atomic charges of the dihydrazone atoms were estimated by Mulliken population analysis applying the DFT/B3LYP levels with the 6-311G(d,p) basis set in gas phase and the result has been listed in **Supl. 6** and has been shown in **Supl. 7**. The atomic charge play a major role in the application of quantum chemical calculations of molecular system due to the atomic charge affect polarizability, electronic structure, dipole moment vibrational spectra, and more properties for a molecular system [91]. The data acquired by Mulliken analysis demonstrated that the atoms of hydrogen have positive charges in 0.083084-0.233649 a.u. because they lose electrons to the neighboring carbon atoms, but H15 has a maximum positive charge than the other hydrogen atoms, which may be due to the attachment of this hydrogen atom to the electronegative atom (N14). The nitrogen and oxy-

Table 5
The effect data of prepared compounds against (concentration used 1mg/mL of DMSO) against *E. coli*, *P. aeruginosa*, *K. pneumonia* and *B. subtilis*.

Compounds	Inhibition zone (IZ, mm) and Activity Index (AI, %)							
	E. coli		*P. aeruginosa*		*B. subtilis*		*K. pneumonia*	
	IZ(mm)	AI (%)	IZ(mm)	AI (%)	IZ(mm)	AI (%)	IZ(mm)	AI (%)
DMSO	–	–			–	–		
Tc	33	100%	40	100%	36	100%	38	100%
HL(1)	25	76%	16	40%	18	50%	15	39%
Mn^{2+}Complex (2)	20	61%	23	58%	17	47%	18	47%
Co^{2+}Complex (3)	21	64%	20	50%	19	53%	20	53%
Ni^{2+}Complex (4)	25	76%	26	65%	19	53%	15	39%
Cu^{2+}Complex (5)	20	61%	17	43%	22	61%	23	61%
Cu^{2+}Complex (6)	26	79%	19	48%	26	72%	25	66%
Zn^{2+}Complex (7)	30	91%	27	68%	22	61%	21	55%
Ru^{3+}Complex (8)	22	67%	19	48%	20	56%	23	61%

gen atoms have a negatively Mulliken charge indicating that these atoms behaved as electron recipients. The carbon atoms are negatively charged except C1, C3, C7, C8, C21, C22 and C32 which may be due to the connection of these carbon atoms to nitrogen and oxygen atoms [92].

3.6.3. Electrostatic potential (ESP) and Molecular electrostatic potential (MEP) analyses

The charge distributions and visualizing variably charged regions for the of dihydrazone **(HL)** molecule was achieved by reviewing the molecular electrostatic potential (MEP) and electrostatic potential (ESP) via DFT calculation (Fig. 6). MEP is commonly utilized as a reactivity map to recognize the hydrogen bonding interactions on organic molecules as well as the sites of nucleophilic and electrophilic reactions [91,93]. MEP, V(r) at a specified point r(x, y, z) in the vicinity of a molecule, is specified in terms of the energy interaction between the electrical charge generated from the molecule's electrons and nuclei and a positive test charge (a proton) located at r. For the system studied the V(r) value has been calculated by the next equation [91].

$$V(r) = \sum_{A} \frac{Z_A}{R_A - r} \int \frac{(r)}{(r - r)} d(r)$$

where, Z_A is the nucleus A charge, situated R_A, $\rho(r')$ denotes to the molecule electronic density function and r' refers to the dummy integration variable [94]. In the MEP, the various values of the electrostatic potential at the surface are symbolized by various colors (from red to blue). The electron rich area, electropositive sites and zero electrostatic potentials areas are symbolized by red, blue green colors, respectively. To expect the effective sites of electrophilic and nucleophilic attacks for dihydrazone **(HL),** the 3D plots of MEP and ESP of dihydrazone **(HL),** utilizing the DFT/B3LYP/6–311G(d,p) method are shown in Fig. 8. As illustrated in this Fig. the MEP of the dihydrazone **(HL),** shows that the highest positive potential area (blue) concentrated on the hydrogen atoms and some carbons atoms with values ranged from +0.083084 to 0.0.465996 a.u., pointing to the probable sites for nucleophilic attack while the highest negative potential sites concentrated on the electronegative atoms (oxygen and nitrogen) make it to the favored sites for chelation with metallic ions. These sites offer info about the location in which the inter-molecular interactions may be formed. From these finding, it may be concluded that the nitrogen and oxygen atoms are the sites of the strongest repulsion while hydrogen atoms are the sites of the strongest attraction. It is clear from the ESP shown in Fig. 8, the negative ESP (colored in red shades) is focused on the molecule except the hydrogen atoms and is manifested as a yellowish blob**.**

3.7. Thermogravimetric analysis

The thermogravimetric data of complexes **(2-8)** in the temperature ranged from room temperature to 1000°C with a rate of heating 10°C/min **(Supl. 8)** were listed in Table 4. The complexes showed three or four decomposition steps in the temperature ranged from 25 to 730°C with total weight loss of ranged from 78.96-88.17% (calcd. 77.29-88.35%) leaving residue of metal oxide or metal oxide polluted by carbon atoms. The thermogram of Mn^{2+}, Co^{2+}, Ni^{2+}, Cu^{2+} and Ru^{3+} complexes **(2-5)** and **(7-8)** showed four decomposition steps which explained as follow, Firstly, the dehydration process within the temperature ranged from 25–150°C which was related to the losing of one or three hydrated water molecules with weight loss of 2.83-8.66% (calcd. 2.99-8.56%). Secondly the liberation of two or one molecules of coordinated water within the temperature ranged from 70–225°C with weight loss of 3.78-6.78% (calcd. 2.99-6.14%). Thirdly, the elimination of two acetate ions or three chloride ions within temperature ranged from 170–400°C with weight loss of 17.82-20.75% (calcd. 17.64-20.27%). The last steps within the temperature ranged from 280–730°C were related to complete decomposition of the molecule with mass loss of 49.06 -57.72% (calcd. 49.86-58.76%). The thermograms of the Cu^{2+} complex **(6)** showed three decomposition steps which explained as follow: firstly, dehydration process at 25–70°C which was related to the losing of two hydrated water molecules with weight loss of 4.47% (calcd. 4.05%). Secondly the elimination of two chloride ions and two phenyl rings at 180-320°C with weight loss equal to 25.98% (calcd. 25.54%). The last step at 320-600°C was allocated to complete decomposition of the complex molecule with mass loss equal to 57.72% (calcd. 58.76%).

3.8. In-vitro *antibacterial study*

The in-vitro antibacterial study of the dihydrazone **(HL, 1)** and its uni-metallic complexes **(2-8)** has been examined against *E. coli*, *P. aeruginosa*, *K. pneumonia* and *B. subtilis* based on agar well diffusion method and has been evaluated via the diameter of inhibition zone. The result of in-vitro antibacterial has been listed in Table 5 and displayed graphically in Fig. 7. The in-vitro antibacterial results demonstrated that the dihydrazone **(1)** has a moderate effect against *E. coli* and a low effect against *P. aeruginosa, K. pneumonia* and *B. subtilis.* The highest activity was found for Zn^{2+} complex against gram-negative strains *E. coli* and *P. aeruginosa* with IZ equal to 30 and 27 mm with AI equal 91 and 68% respectively. The lowest effect against gram negative strains *E. coli* and *P. aeruginosa* was noted for Cu^{2+} complex **(5)** with IZ equal to 16 and 17 mm and AI equal 48 and 43%. In case of gram-positive strains *K. pneumonia* and *B. subtilis* the highest activity was found for Cu^{2+} complex **(6)** with IZ equal to 25 and 26 mm with AI equal 72 and

66% respectively. While the Ni^{2+} and Mn^{2+}complexes showed the lowest activity against the two strains respectively with IZ equal to 15 and 17 mm and AI equal 39 and 47% respectively. The enhancement of the antibacterial activity of some complexes may also be clarified based on the chelation theory, because of the alteration in the metallic ions polarization which leading to the modification of the complex's lipophilicity. The action mechanism of antibacterial effect of chelated compounds may be attributed to the increasement in the lipophilic character of the complexes resulting from chelation. Chelating process diminishes the polarity of the metallic ions mainly due to the partial sharing of their positive charge with the donor atoms as well as probable π-electron delocalization in the whole chelating ring. The chelation also raises the lipophilic character of the central metallic ions, which consequently favors the penetration via the cell membrane lipid layer so inhibit the bacterial wall synthesis or activate enzymes that destroy the cell wall. The action mode of complexes may also involve the hydrogen bonds formation with the imino group by the active sites that will lead to interfering with the synthesis of cell wall [95]. The hydrogen bond formation is leading to damage the cytoplasmic membrane and the cell permeability may also be altered leading to cell death.

The orders of antibacterial of the dihydrazone and its chelated compounds against *E. coli* was found to be Tc>Zn^{2+}**(7)**>Cu^{2+}(**6**)>Ni^{2+}**(4)=**HL(**1**)>Ru^{3+}(**8**)>Co^{2+}(**3**)>Mn^{2+}(**2**)>Cu^{2+}(**5**), against *P. aeruginosa* is found to be Tc>Zn^{2+}**(7)**>Ni^{2+}**(4)**>Co^{2+} (**3**)>Mn^{2+}**(2)** =Cu^{2+}(**6**)=Ru^{3+}**(8)**> Cu^{2+}**(5)>**HL(**1**), against *K. pneumonia* was found to be Tc>Cu^{2+}(**6**)>Cu^{2+}(**5**)=Ru^{3+}**(8)** **>**Zn^{2+}**(7)**> Co^{2+}**(3)**>Mn^{2+}**(2)>**HL**(1)=**Ni^{2+}**(4)** and against *B. subtilis* was found to be Tc>Cu^{2+}(**6**)>Cu^{2+}(**5**)= Zn^{2+}**(7)**>Ru^{3+}**(8)>**Co^{2+}**(3)=**Ni^{2+}**(4)>**HL(**1**)>Mn^{2+}**(2)**. Furthermore, the activities of the prepared dihydrazone and its metallic complexes were reinforced by determining the index of activity in accordance to the published equation [57], and then were displayed in (Figs. 8 & 9). The index of activity confirms the fact that Cu^{2+} and Zn^{2+} complexes **(6-7)** had higher activity index than others complexes and the parent dihydrazone against gram-positive and gram-negative, respectively. The difference in antibacterial activity of may be due to the nature of microorganism's cell membrane and metal ions. The higher activity of some complexes in comparing with that of the free dihydrazone may be because of the reduction in the charge localization of the metallic ions that leading to the greater lipid solubility [96,97].

4. Conclusion

The dihydrazone, 3-(-(1,5-dimethyl-3-oxo-2-phenyl-2,3-dihydro-1H-pyrazol-4-yl) methylene)hydrazono)indolin-2-one (HL) and its uni-metallic chelated compounds of Ru^{3+}, Co^{2+}, Ni^{2+}, Cu^{2+} and Zn^{2+} have been synthesized and separated with a conventional refluxing strategy. The FT-IR, ^{1}H- and ^{13}C-NMR spectroscopic data has shown that the dihydrazone behaved as a neutral bidentate chelator coordinated with metallic cations via oxygen and nitrogen atoms of carbonyl and azomethine groups of the isatin moiety. The calculated and experimental element percentages reveals that the isolated chelated compounds are composed in 1M:1L molar ratio. The EAS and magnetic moments results displayed that the complexes **(2-8)** have a distorted or regular octahedral geometry. TG study signaled that the complexes degraded in four or three overlapping stages starting with dehydration process and ending with complete degradation of the complexes leaving the related metal oxide contaminated by carbon residue. The antibacterial activity of the prepared compounds which assessed by agar well diffusion method versus *E. coli, P. aeruginosa, K. pneumonia* and *B. subtilis* demonstrated that the Zn^{2+} complex **(7)** has activity more than the parent dihydrazone and other complexes against gram-negative bacteria while the Cu^{2+} complex **(6)** is more active against gram-positive bacteria.

Funding statement

This work was funded by the Deanship of Scientific Research (DSR) University of Jeddah, Jeddah, Saudi Arabia under grant no (UJ-02-055-DR).

Data availability statement

The data that supports the findings of this study are available in the supplementary material of this article.

Credit author statement

All authors conceived and designed the experiments, performed the experiments, analyzed the data, contributed reagents/materials/analysis tools, wrote the paper, reviewed drafts of the paper. All authors read and approved the final manuscript.

Declaration of Competing Interest

The authors declare that they have no known competing financial interests or personal relationships that could have appeared to influence the work reported in this paper.

Supplementary materials

Supplementary material associated with this article can be found, in the online version, at doi:10.1016/j.molstruc.2021.131194.

References

[1] N. Kerru, L. Gummidi, S. Maddila, K.K. Gangu, S.B. Jonnalagadda, A review on recent advances in nitrogen-containing molecules and their biological applications, Molecules 25 (8) (2020) 1909.

[2] P.K. Sharma, A. Amin, M. Kumar, A Review, Medicinally important nitrogen sulphur containing heterocycles, Open Med. Chem. J. 14 (2020) 49–64.

[3] S. Abdpour, L. Jalili-Baleh, H. Nadri, H. Forootanfar, S.N.A. Bukhari, A. Ramazani, S.E.S. Ebrahimi, A. Foroumadi, M. Khoobi, Chromone derivatives bearing pyridinium moiety as multi-target-directed ligands against Alzheimer's disease, Bioorg. Chem. 110 (2021) 104750.

[4] R. Alikhani, N. Razzaghi-Asl, A. Ramazani, Z. Hosseinzadeh, Insights into the structural/conformational requirements of cytotoxic oxadiazoles as potential chemotherapeutic target binding agents, J. Mol. Struct. 1164 (2018) 9–22.

[5] A. Ramazani, M. Khoobi, A. Torkaman, F. Zeinali Nasrabadi, H. Forootanfar, M. Shakibaie, M. Jafari, A. Ameri, S. Emami, M.A. Faramarzi, A. Foroumadi, A. Shafiee, One-pot, four-component synthesis of novel cytotoxic agents 1-(5-aryl-1,3,4-oxadiazol-2-yl)-1-(1H-pyrrol-2-yl)methanamines, Eur. J. Med. Chem. 78 (2014) 151–156.

[6] M. Azizmohammadi, M. Khoobi, A. Ramazani, S. Emami, A. Zarrin, O. Firuzi, R. Miri, A. Shafiee, 2H-chromene derivatives bearing thiazolidine-2,4-dione, rhodanine or hydantoin moieties as potential anticancer agents, Eur. J. Med. Chem. 59 (2013) 15–22.

[7] M. Khoobi, S. Emami, G. Dehghan, A. Foroumadi, A. Ramazani, A. Shafiee, Synthesis and Free Radical Scavenging Activity of Coumarin Derivatives Containing a 2-Methylbenzothiazoline Motif, Arch. Pharm. Chem. Life Sci. 344 (9) (2011) 588–594.

[8] M. Khoobi, A. Foroumadi, S. Emami, M. Safavi, G. Dehghan, B.H. Alizadeh, A. Ramazani, S.K. Ardestani, A. Shafiee, Coumarin-Based Bioactive Compounds: Facile Synthesis and Biological Evaluation of Coumarin-Fused 1,4-Thiazepines, Chem. Biol. Drug. Des. 78 (4) (2011) 580–586.

[9] M.S. Çavuş, H. Yakan, H. Muğlu, T. Bakır, Novel carbohydrazones including 5-substituted isatin: Synthesis, characterization, and quantum-chemical studies on the relationship between electronic and antioxidant properties, J. Phys. Chem. Solids 140 (2020) 109362.

[10] F.A. Khan, A. Maalik, Advances in Pharmacology of Isatin and its Derivatives: A Review, Trop. J. Pharm. Res. 14 (10) (2015) 1937–1942.

[11] X.-M. Zhang, H. Guo, Z.-S. Li, F.-H. Song, W.-M. Wang, H.-Q. Dai, L.-X. Zhang, J.-G. Wang, Synthesis and evaluation of isatin-β-thiosemicarbazones as novel agents against antibiotic-resistant Gram-positive bacterial species, Eur. J. Med. Chem. 101 (2015) 419–430.

[12] H. Guo, Isatin derivatives and their anti-bacterial activities, Eur. J. Med. Chem. 164 (2019) 678–688.

[13] A.V. Bogdanov, I.F. Zaripova, A.D. Voloshina, A.S. Sapunova, N.V. Kulik, I.V. Tsivunina, A.B. Dobrynin, V.F. Mironov, Isatin derivatives bearing a fluorine atom. Part 1: Synthesis, hemotoxicity and antimicrobial activity evaluation of fluoro-benzylated water-soluble pyridinium isatin-3-acylhydrazones, Journal of Fluorine Chemistry 227 (2019) 109345.

[14] C.S. Marques, Ó. López, D. Bagetta, E.P. Carreiro, S. Petralla, M. Bartolini, M. Hoffmann, S. Alcaro, B. Monti, M.L. Bolognesi, M. Decker, J.G. Fernández-Bolaños, A.J. Burke, N-1,2,3-triazole-isatin derivatives for cholinesterase and β-amyloid aggregation inhibition: A comprehensive bioassay study, Bioorg. Chem. 98 (2020) 103753.

[15] Y.A. Ammar, A.M. Sh El-Sharief, A. Belal, S.Y. Abbas, Y.A. Mohamed, A.B.M. Mehany, A. Ragab, Design, synthesis, antiproliferative activity, molecular docking and cell cycle analysis of some novel (morpholinosulfonyl) isatins with potential EGFR inhibitory activity, Eur. J. Med. Chem. 156 (2018) 918–932.

[16] E. Bulatov, R. Sayarova, R. Mingaleeva, R. Miftakhova, M. Gomzikova, Y. Ignatyev, A. Petukhov, P. Davidovich, A. Rizvanov, N.A. Barlev, Isatin-Schiff base–copper (II) complex induces cell death in p53-positive tumors, Cell Death Discovery 4 (1) (2018) 103.

[17] G. Wang, M. Chen, J. Qiu, Z. Xie, A. Cao, Synthesis, in vitro α-glucosidase inhibitory activity and docking studies of novel chromone-isatin derivatives, Bioorg. Med. Chem. Lett. 28 (2) (2018) 113–116.

[18] K.R. Ansari, M.A. Quraishi, A. Singh, Isatin derivatives as a non-toxic corrosion inhibitor for mild steel in 20% H2SO4, Corros. Sci. 95 (2015) 62–70.

[19] C.Justin Dhanaraj, J. Johnson, DNA interaction, antioxidant and in vitro cytotoxic activities of some mononuclear metal(II) complexes of a bishydrazone ligand, Materials Science and Engineering: C 78 (2017) 1006–1015.

[20] H.S. Ibrahim, S.M. Abou-Seri, N.S.M. Ismail, M.M. Elaasser, M.H. Aly, H.A. Abdel-Aziz, Bis-isatin hydrazones with novel linkers: Synthesis and biological evaluation as cytotoxic agents, Eur J Med Chem 108 (2016) 415–422.

[21] R. Fouad, O.M.I. Adly, Novel Cu2+ and Zn2+ nanocomplexes drug based on hydrazone ligand bearings chromone and triazine moieties: Structural, spectral, DFT, molecular docking and cytotoxic studies, J. Mol. Struct. 1225 (2021) 129158.

[22] Y.P. Singh, S.K. Patel, Molecular structures, spectral, electrochemical, DFT and antioxidant activities of copper(II) complexes with NNO donor Schiff base ligand, J. Mol. Struct. 1228 (2021) 129457.

[23] A. Zülfikaroğlu, Ç. Yüksektepe Ataol, E. Çelikoğlu, U. Çelikoğlu, Ö. İdil, New Cu(II), Co(III) and Ni(II) metal complexes based on ONO donor tridentate hydrazone: Synthesis, structural characterization, and investigation of some biological properties, J. Mol. Struct. 1199 (2020) 127012.

[24] S.S. Swathy, R. Selwin Joseyphus, V.P. Nisha, N. Subhadrambika, K. Mohanan, Synthesis, spectroscopic investigation and antimicrobial activities of some transition metal complexes of a [(2-hydroxyacetophenone)-3-isatin]-bishydrazone, Arab. J. Chem. 9 (2016) S1847–S1857.

[25] J. Devi, N. Batra, Synthesis, characterization and antimicrobial activities of mixed ligand transition metal complexes with isatin monohydrazone Schiff base ligands and heterocyclic nitrogen base, Spectrochim. Acta Part A Mol. Biomol. Spectrosc. 135 (2015) 710–719.

[26] C.S. Rocha, L.F.O.B. Filho, A.E. de Souza, R. Diniz, Â.M.L. Denadai, H. Beraldo, L.R. Teixeira, Structural studies and investigation on the antifungal activity of silver(I) complexes with 5-nitrofuran-derived hydrazones, Polyhedron 170 (2019) 723–730.

[27] J. McNulty, C. Babu Dokuburra, L. D'Aiuto, M. Demers, L. McClain, P. Piazza, K. Williamson, W. Zheng, V.L. Nimgaonkar, Synthesis of non-nucleoside anti-viral cyclopropylcarboxacyl hydrazones and initial anti-HSV-1 structure-activity relationship studies, Bioorg. Med. Chem. Lett. 30 (24) (2020) 127559.

[28] Z. Peng, G. Wang, Q.-H. Zeng, Y. Li, Y. Wu, H. Liu, J.J. Wang, Y. Zhao, Synthesis, antioxidant and anti-tyrosinase activity of 1,2,4-triazole hydrazones as antibrowning agents, Food Chem 341 (2021) 128265.

[29] S. Khan, M. Tariq, M. Ashraf, S. Abdullah, M. al-Rashida, M. Khalid, P. Taslimi, M. Fatima, R. Zafar, Z. Shafiq, Probing 2-acetylbenzofuran hydrazones and their metal complexes as α-glucosidase inhibitors, Bioorg. Chem. 102 (2020) 104082.

[30] G. Verma, A. Marella, M. Shaquiquzzaman, M. Akhtar, M.R. Ali, M.M. Alam, A review exploring biological activities of hydrazones, Journal of Pharmacy and Bioallied Sciences 6 (2) (2014) 69–80.

[31] s. Hussain, A. Ali, Exploring the Pharmacological Activities of Hydrazone Derivatives: A Review, J. Phytochemistry Biochem. 1 (1) (2017) 104–108.

[32] D. Kuriakose, M.R.P. Kurup, Mononuclear and binuclear dioxidomolybdenum(VI) complexes of ONO appended aroylhydrazone: Crystal structures, interaction energy calculation and cytotoxicity, J. Mol. Struct. 1204 (2020) 127467.

[33] D.C. Santos, R.R. Henriques, M.A.d.A.L. Junior, A.B. Farias, T.L.d.C. Nogueira, J.V.F. Quimas, N.C. Romeiro, L.L.d. Silva, A.L.F.d. Souza, Acylhydrazones as isoniazid derivatives with multi-target profiles for the treatment of Alzheimer's disease: Radical scavenging, myeloperoxidase/acetylcholinesterase inhibition and biometal chelation, Bioorg. Med. Chem. 28 (10) (2020) 115470.

[34] Z. You, H. Yu, Z. Li, W. Zhai, Y. Jiang, A. Li, S. Guo, K. Li, C. Lv, C. Zhang, Inhibition studies of Jack bean urease with hydrazones and their copper(II) complexes, Inorg. Chim. Acta 480 (2018) 120–126.

[35] R. Fekri, M. Salehi, A. Asadi, M. Kubicki, Synthesis, characterization, anticancer and antibacterial evaluation of Schiff base ligands derived from hydrazone and their transition metal complexes, Inorg. Chim. Acta 484 (2019) 245–254.

[36] S. Layek, B. Agrahari, A. Kumar, N. Dege, D.D. Pathak, Synthesis and X-ray crystal structures of three new nickel(II) complexes of benzoylhydrazones: Catalytic applications in the synthesis of 2-arylbenzoxazoles, Inorg. Chim. Acta 500 (2020) 119222.

[37] M.S.S. Adam, K.A. Soliman, H.M. Abd El-Lateef, Homo-dinuclear VO2+and Ni2+dihydrazone complexes: Synthesis, characterization, catalytic activity and CO2-corrosion inhibition under sustainable conditions, Inorg. Chim. Acta 499 (2020) 119212.

[38] F.A. El-Saied, T.A. Salem, M.M.E. Shakdofa, A.N. Al-Hakimi, Anti-neurotoxic evaluation of synthetic and characterized metal complexes of thiosemicarbazone derivatives, Appl. Organomet. Chem. 32 (4) (2018) e4215.

[39] M.M.E. Shakdofa, H.A. Mousa, A.M.A. Elseidy, A.A. Labib, M.M. Ali, A.S. Abd-El-All, Anti-proliferative activity of newly synthesized Cd(II), Cu(II), Zn(II),Ni(II), Co(II), VO(II), and Mn(II) complexes of 2-((4,9-dimethoxy-5-oxo-5H-furo[3,2-g]chromen-6-yl)methylene) hydrazinecarbothioamide on three human cancer cells, Appl. Organomet. Chem. 32 (1) (2018) e3936.

[40] F.A. El-Saied, T.A. Salem, S.A. Aly, M.M.E. Shakdofa, Evaluation of Anti-Hyperglycemic Effect of Synthetic Schiff Base Vanadium(IV) Complexes, Pharm. Chem. J. 51 (9) (2017) 833–842.

[41] M.M.E. Shakdofa, H.A. Mousa, A.A. Labib, A.S. Abd-El-All, A.A. El-Beih, M.M. Abdalla, Synthesis and characterization of novel chromone Schiff base complexes as p53 activators, Appl. Organomet. Chem. 32 (6) (2018) e4345.

[42] M.M.E. Shakdofa, A.A. Labib, N.A. Abdel-Hafez, H.A. Mousa, Synthesis and Characterization of VO^{2+}, Co^{2+}, Ni^{2+}, Cu^{2+} and Zn^{2+} Complexes of a Schiff base ligand derived from ethyl 2-amino-6-ethyl-4,5,6,7-tetrahydrothieno[2,3-c]pyridine-3-carboxylate and their Investigation as fungicide Agents, Appl. Organomet. Chem. 32 (12) (2018) e4581.

[43] M.M.E. Shakdofa, F.A. El-Saied, A.J. Rasras, A.N. Al-Hakimi, Transition metal complexes of a hydrazone–oxime ligand containing the isonicotinoyl moiety: Synthesis, characterization and microbicide activities, Appl. Organomet. Chem. 32 (7) (2018) e4376.

[44] F.A. El-saied, M.M.E. Shakdofa, A.N. Al-Hakimi, A.M.E. Shakdofa, Transition metal complexes derived from N′-(4-fluorobenzylidene)-2-(quinolin-2-yloxy) acetohydrazide: Synthesis, structural characterization, and biocidal evaluation, Appl. Organomet. Chem. 34 (11) (2020) e5898.

[45] M.M.E. Shakdofa, N.A. Morsy, A.J. Rasras, A.N. Al-Hakimi, A.M.E. Shakdofa, Synthesis, characterization, and density functional theory studies of hydrazone–oxime ligand derived from 2,4,6-trichlorophenyl hydrazine and its metal complexes searching for new antimicrobial drugs, Appl. Organomet. Chem. 35 (2) (2021) e6111.

[46] A.I. Vogel, in: Vogle's Text Book of Quantitative chemical Analysis, JOHN WIELY & SONS New York, 1989, p. 906.

[47] G. Svehla, Vogel's textbook of macro and semi micro Quantitative inorganic analysis, 5th ed., Longman Inc., New York, 1979.

[48] S.M. Emam, D.A. Tolan, A.M. El-Nahas, Synthesis, structural, spectroscopic, and thermal studies of some transition-metal complexes of a ligand containing the amino mercapto triazole moiety, Appl. Organomet. Chem. 34 (5) (2020) e5591.

[49] L. Lewis, R.G. Wilkins, Modern Coordination Chemistry, Interscience, New York, 1960.

[50] R.K. Boggess, D.A. Zatko, The use of conductivity data for the structure determination of metal complexes, J. Chem. Educ. 52 (10) (1975) 649.

[51] M.J. Frisch, G.W. Trucks, H.B. Schlegel, G.E. Scuseria, M.A. Robb, J.R. Cheeseman, G. Scalmani, V. Barone, G.A. Petersson, H. Nakatsuji, X. Li, M. Caricato, A. Marenich, J. Bloino, B.G. Janesko, R. Gomperts, B. Mennucci, H.P. Hratchian, J.V. Ortiz, A.F. Izmaylov, J.L. Sonnenberg, D. Williams-Young, F. Ding, F. Lipparini, F. Egidi, J. Goings, B. Peng, A. Petrone, T. Henderson, D. Ranasinghe, V.G. Zakrzewski, N.R.J. Gao, G. Zheng, W. Liang, M. Hada, M. Ehara, K. Toyota, R. Fukuda, J. Hasegawa, M. Ishida, T. Nakajima, Y. Honda, O. Kitao, H. Nakai, T. Vreven, K. Throssell, J.A. Montgomery Jr., J.E. Peralta, F. Ogliaro, M. Bearpark, J.J. Heyd, E. Brothers, K.N. Kudin, V.N. Staroverov, R.T. Keith, J.Normand Kobayashi, K. Raghavachari, A. Rendell, J.C. Burant, S.S. Iyengar, J. Tomasi, M. Cossi, J.M. Millam, M. Klene, C. Adamo, R. Cammi, J.W. Ochterski, R.L. Martin, K. Morokuma, O. Farkas, J.B. Foresman, D.J. Fox, Gaussian 09, Revision A02, Gaussian, Inc, Wallingford CT, 2016.

[52] T. Keith, J. Millam, GaussView, Version 5.0.9, Semichem. Inc., Mission, KS, 2009.

[53] A.D. Becke, Density-functional thermochemistry. III, The role of exact exchange 98 (7) (1993) 5648–5652.

[54] C. Lee, W. Yang, R.G. Parr, Development of the Colle-Salvetti correlation-energy formula into a functional of the electron density, Phys. Rev. B 37 (2) (1988) 785–789.

[55] J. Collee, J. Duguid, A. Fraser, B. Marmion, Mackie and McCartney Practical Medical Microbiology, 5th edition, Churchill Livingstone, Longman groups U. KLtd, 1989.

[56] I.A. Holder, S.T. Boyce, Agar well diffusion assay testing of bacterial susceptibility to various antimicrobials in concentrations non-toxic for human cells in culture, Burns 20 (5) (1994) 426–429.

[57] R.R. Zaky, K.M. Ibrahim, I.M. Gabr, Bivalent transition metal complexes of o-hydroxyacetophenone [N-(3-hydroxy-2-naphthoyl)] hydrazone: Spectroscopic, antibacterial, antifungal activity and thermogravimetric studies, Spectrochim. Acta Part A Mol. Biomol. Spectrosc. 81 (1) (2011) 28–34.

[58] W.J. Geary, The use of conductivity measurements in organic solvents for the characterisation of coordination compounds, Coord. Chem. Rev. 7 (1) (1971) 81–122.

[59] L.H. Abdel-Rahman, A.M. Abu-Dief, H. Moustafa, S.K. Hamdan, Ni(II) and Cu(II) complexes with ONNO asymmetric tetradentate Schiff base ligand: synthesis,

spectroscopic characterization, theoretical calculations, DNA interaction and antimicrobial studies, Appl. Organomet. Chem. 31 (2) (2017) e3555.

[60] S.S. Kumar, S. Biju, V. Sadasivan, Synthesis, structure characterization and biological studies on a new aromatic hydrazone, 5-(2-(1,5-dimethyl-3-oxo-2-phenyl-2,3-dihydro-1H-pyrazol-4-yl)hydrazono)-2,2-dimethyl-1,3-dioxane-4,6-dione, and its transition metal complexes, J. Mol. Struct. 1156 (2018) 201–209.

[61] M.F.R. Fouda, M.M. Abd-Elzaher, M.M.E. Shakdofa, F.A. El Saied, M.I. Ayad, A.S. El Tabl, Synthesis and characterization of transition metal complexes of N′-[(1,5-dimethyl-3-oxo-2-phenyl-2,3-dihydro-1H-pyrazol-4-yl)methylene] thiophene-2-carbohydrazide, Transition Met. Chem. 33 (2) (2008) 219–228.

[62] I.S. Butler, S.A. Elsayed, A.M. El-Hendawy, S.I. Mostafa, B.J. Jean-Claude, M. Todorova, Antineoplastic activity of new transition metal complexes of 6-methylpyridine-2-carbaldehyde-n(4)-ethylthiosemicarbazone: X-Ray crystal structures of [VO2 (mpETSC)] and [Pt(mpETSC)Cl], Bioinorg. Chem. Appl. 2010 (2010).

[63] L.P. Nitha, R. Aswathy, N.E. Mathews, B. Sindhu kumari, K. Mohanan, Synthesis, spectroscopic characterisation, DNA cleavage, superoxidase dismutase activity and antibacterial properties of some transition metal complexes of a novel bidentate Schiff base derived from isatin and 2-aminopyrimidine, Spectrochim. Acta Part A Mol. Biomol. Spectrosc. 118 (2014) 154–161.

[64] Z.H.A. El-Wahab, M.M. Mashaly, A.A. Salman, B.A. El-Shetary, A.A. Faheim, Ce(III) and UO$_2$(VI) bis-salicylatothiosemicarbazide complexes: Binary and ternary complexes, thermal studies and antimicrobial activity, Spectrochim. Acta Part A Mol. Biomol. Spectrosc. 60 (12) (2004) 2861–2873.

[65] K. Nakamoto, Infrared and Raman Spectra of Inorganic and Coordination Compounds Part B: Applications in Coordination, Organometallic, and Bioinorganic Chemistry, 6th ed., John Wiley & Sons INC, USA, 2009.

[66] A.S. El-Tabl, M.M.E. Shakdofa, M.A. Whaba, Synthesis, characterization and fungicidal activity of binary and ternary metal(II) complexes derived from 4,4′-((4-nitro-1,2-phenylene) bis(azanylylidene))bis(3-(hydroxyimino)pentan-2-one), Spectrochim. Acta Part A Mol. Biomol. Spectrosc. 136 (PC) (2015) 1941–1949.

[67] M.M. Makhlouf, H.A. Alburaih, M.M. Shehata, M.S.S. Adam, M.M. Mostafa, A. El-Denglawey, Synthesis, physicochemical and optical characterizations of a new isatin hydrazone derivative and its ZnO-complex for potential energy conversion and storage applications, J. Phys. Chem. Solids 151 (2021) 109817.

[68] O.A. Dar, S.A. Lone, M.A. Malik, F.M. Aqlan, M.Y. Wani, A.A. Hashmi, A. Ahmad, Synthesis and synergistic studies of isatin based mixed ligand complexes as potential antifungal therapeutic agents, Heliyon 5 (7) (2019) e02055.

[69] R. Sharma, S.K. Agarwal, S. Rawat, M. Nagar, Synthesis, Characterization and Antibacterial Activity of Some Transition Metal cis-3,7-dimethyl-2,6-octadiensemicarbazone Complexes, Transition Met. Chem. 31 (2) (2006) 201–206.

[70] N.A. Mangalam, S.R. Sheeja, M.R.P. Kurup, Mn(II) complexes of some acylhydrazones with NNO donor sites: Syntheses, a spectroscopic view on their coordination possibilities and crystal structures, Polyhedron 29 (18) (2010) 3318–3323.

[71] A.B.P. Lever, Inorganic electronic spectroscopy, Elsevier science, Amsterdam, 1984.

[72] D.N. Sathyanarayana, Electronic Absorption Spectroscopy and Related Techniques, Universities Press, 2001.

[73] E. Katsoulakou, V. Bekiari, C.P. Raptopoulou, A. Terzis, P. Lianos, E. Manessi-Zoupa, S.P. Perlepes, Dinuclear versus tetranuclear cluster formation in zinc(II) nitrate/di-2-pyridyl ketone chemistry: Synthetic, structural and spectroscopic studies, Spectrochim. Acta Part A Mol. Biomol. Spectrosc. 61 (7) (2005) 1627–1638.

[74] A.S. El-Tabl, M.M.E. Shakdofa, B.M. Herash, Antibacterial activities and spectroscopic characterization of synthetic metal complexes of 4-(3-(hydroxyimino)-4-oxopentan-2-ylidene)amino)-1,5- dimethyl-2-phenyl-1H-pyrazol-3(2H)-one, Main Group Chem 12 (3) (2013) 257–274.

[75] C. Anitha, C.D. Sheela, P. Tharmaraj, S.Johnson Raja, Synthesis and characterization of VO(II), Co(II), Ni(II), Cu(II) and Zn(II) complexes of chromone based azo-linked Schiff base ligand, Spectrochim. Acta Part A Mol. Biomol. Spectrosc. 98 (2012) 35–42.

[76] M. Shebl, Mononuclear, homo- and hetero-binuclear complexes of 1-(5-(1-(2-aminophenylimino)ethyl)-2,4-dihydroxyphenyl)ethanone: Synthesis, magnetic, spectral, antimicrobial, antioxidant, and antitumor studies, J. Coord. Chem. 69 (2) (2016) 199–214.

[77] S.L. Reddy, T. Endo, G.S. Reddy, Electronic (Absorption) Spectra of 3d Transition Metal Complexes, Advanced Aspects of Spectroscopy, InTech (2012).

[78] S. Chandra, L.K. Gupta, EPR and electronic spectral studies on Co(II), Ni(II) and Cu(II) complexes with a new tetradentate [N4] macrocyclic ligand and their biological activity, Spectrochim. Acta Part A Mol. Biomol. Spectrosc. 60 (7) (2004) 1563–1571.

[79] S. Chandra, S. Gautam, H.K. Rajor, R. Bhatia, Syntheses, spectroscopic characterization, thermal study, molecular modeling, and biological evaluation of novel Schiff's base benzil bis(5-amino-1,3,4-thiadiazole-2-thiol) with Ni(II), and Cu(II) metal complexes, Spectrochim. Acta Part A Mol. Biomol. Spectrosc. 137 (2015) 749–760.

[80] A.A. El-Bindary, A.Z. El-Sonbati, Synthesis and properties of complexes of Copper(II), Nickel(II), Cobalt(II) and uranyl ions with 3-(p-Tolylsulphonamido)rhodanine, Polish J. Chem. 74 (5) (2000) 615–620.

[81] M.F.R. Fouda, M.M. Abd-Elzaher, M.M. Shakdofa, F.A. El-Saied, M.I. Ayad, A.S. El Tabl, Synthesis and characterization of a hydrazone ligand containing antipyrine and its transition metal complexes, J. Coord. Chem. 61 (12) (2008) 1983–1996.

[82] G. Puthilibai, S. Vasudhevan, S.John Mary, Synthesis, spectral, electrochemical and DNA binding properties of ruthenium (III) complexes of Schiff bases containing N,O donor atoms, Mat. Today: Proc 36 (2021) 809–813.

[83] P. Geerlings, F. De Proft, W. Langenaeker, Conceptual Density Functional Theory, Chem. Rev. 103 (5) (2003) 1793–1874.

[84] T.A. Yousef, O.K. Alduaij, G.M. Abu El-Reash, R.M. El Morshedy, Semiempirical studies, spectral analysis, in vitro antibacterial and DNA degradation studies of heterocyclic thiosemicarbazone ligand and its metal complexes, J. Mol. Liquids 222 (2016) 762–776.

[85] M.S. Masoud, A.E. Ali, M.A. Shaker, G.S. Elasala, Synthesis, computational, spectroscopic, thermal and antimicrobial activity studies on some metal–urate complexes, Spectrochim. Acta Part A Mol. Biomol. Spectrosc. 90 (2012) 93–108.

[86] N. Beyazit, B. Çatıkkaş, Ş. Bayraktar, C. Demetgül, Synthesis, characterization and catecholase-like activity of new Schiff base metal complexes derived from visnagin: Theoretical and experimental study, J. Mol. Struct. 1119 (2016) 124–132.

[87] J.B. Foresman, A. Frisch, Exploring Chemistry With Electronic Structure Methods: A Guide to Using Gaussian, 2nd ed., Gaussian, Pittsburgh, 1996.

[88] Z. Fakhar, T. Govender, G. Lamichhane, G.E.M. Maguire, H.G. Kruger, B. Honarparvar, Computational model for the acylation step of the β-lactam ring: Potential application for l,d-transpeptidase 2 in mycobacterium tuberculosis, J. Mol. Struct. 1128 (2017) 94–102.

[89] M. Sertçelik, Synthesis, spectroscopic properties, crystal structures, DFT studies, and the antibacterial and enzyme inhibitory properties of a complex of Co(II) 3,5-difluorobenzoate with 3-pyridinol, J. Chem. Res. (2020) 44.

[90] M.R. Mlahi, E.M. Afsah, A. Negm, M.M. Mostafa, Synthesis of 8-hydroxyquinolium chloroacetate and synthesis of complexes derived from 8-hydroxyquinoline, and characterization, density functional theory and biological studies, Appl. Organomet. Chem. 29 (4) (2015) 200–208.

[91] A. Eşme, S.G. Sağdınç, Spectroscopic (FT–IR, FT–Raman, UV–Vis) analysis, conformational, HOMO-LUMO, NBO and NLO calculations on monomeric and dimeric structures of 4–pyridazinecarboxylic acid by HF and DFT methods, J. Mol. Struct. 1147 (2017) 322–334.

[92] S.A. Khan, K. Rizwan, S. Shahid, M.A. Noamaan, T. Rasheed, H. Amjad, Synthesis, DFT, computational exploration of chemical reactivity, molecular docking studies of novel formazan metal complexes and their biological applications, Appl. Organomet. Chem. 34 (3) (2020) e5444.

[93] P. Politzer, D.G. Truhlar, Chemical Applications of Atomic and Molecular Electrostatic Potentials:Reactivity, Structure, Scattering, and Energetics of Organic, Inorganic, and Biological Systems, 1st ed., Springer, New York, 1981.

[94] P. Politzer, J.S. Murray, The fundamental nature and role of the electrostatic potential in atoms and molecules, Theor. Chem. Acc. 108 (3) (2002) 134–142.

[95] A.W. Bauer, W.M. Kirby, J.C. Sherris, M. Turck, Antibiotic susceptibility testing by a standardized single disk method, Am. J. Clin. Pathol. 45 (4) (1966) 493–496.

[96] M. Belicchi Ferrari, S. Capacchi, G. Pelosi, G. Reffo, P. Tarasconi, R. Albertini, S. Pinelli, P. Lunghi, Synthesis, structural characterization and biological activity of helicin thiosemicarbazone monohydrate and a copper(II) complex of salicylaldehyde thiosemicarbazone, Inorg. Chim. Acta 286 (2) (1999) 134–141.

[97] R. Selwin Joseyphus, M. Sivasankaran Nair, Synthesis, characterization and biological studies of some Co(II), Ni(II) and Cu(II) complexes derived from indole-3-carboxaldehyde and glycylglycine as Schiff base ligand, Arab. J. Chem. 3 (4) (2010) 195–204.